ChIP-seq Identifies *Lrp6* As a Novel αNAC Gene Target Following PTH Treatment

Julie Ann Miller

Department of Human Genetics

McGill University, Montreal, Quebec, Canada

May 2015

A thesis submitted to McGill University in partial fulfillment of the requirements of the degree of

Master of Science in Human Genetics

To my boys,

“I’ve got everything I need right in front of me”.

-Bret McKenzie

Table of Contents

Abstract

The alpha chain of the nascent polypeptide associated complex (αNAC) functions as a transcriptional coregulator in osteoblasts. When osteoblasts are stimulated by parathyroid hormone (PTH), a PKA-dependent signaling pathway induces αNAC to translocate from the cytoplasm to the nucleus, where it regulates bone-specific gene transcription. Although mutation studies show that intra-nuclear activity of αNAC plays a pivotal role in bone development in mice, few of αNACs transcriptional targets are known. Here, we use the high-throughput sequencing technique ChIP-seq to search across the mouse genome for targets of αNAC. We identify as a novel candidate gene target of αNAC the gene *Lrp6*, which codes for a key component of the Wnt signaling pathway, an important regulator of bone development. Using RNA-seq, we show that PTH treatment induces significant *Lrp6* gene expression in osteoblast cells. ChIP assays confirm that the PTH-induced PKA-mediated phosphorylated form of αNAC at residue serine 99 (S99) binds to the promoter region of *Lrp6.* Finally, shRNA studies in which endogenous αNAC expression is knocked down provoked a significant reduction in *Lrp6* expression. Taken together, these findings point to αNAC as a regulator of *Lrp6* gene expression. In our future research, we aim to determine the specific binding site of αNAC at the promoter of *Lrp6,* and determine its transcriptional activity. Additionally, we will characterize the physiological consequences of αNAC's effects on *Lrp6* expression during bone development, and identify αNAC's involvement in other molecular pathways.

Résumé

La chaîne alpha du dimère NAC (*Nascent polypeptide associated complex*) αNAC, fonctionne comme un élément régulateur transcriptionnel dans les ostéoblastes. Lorsque les ostéoblastes sont stimulés par l'hormone parathyroïdienne (PTH), un mécanisme impliquant l'enzyme PKA induit αNAC à se deplacer du cytoplasme vers le noyau, où il module la transcription génique. Bien que des études sur des animaux transgéniques démontrent qu'αNAC joue un rôle physiologique sur la transcription dans les ostéoblastes, les cibles génétiques d' αNAC sont peu étudiées. Dans notre étude, nous utilisons la technique ChIP-seq pour identifier des cibles potentielles d'αNAC. Nous identifions comme cible d'αNAC le gène *Lrp6*. Ce gène correspond à une protéine qui constitue un élément clé du mécanisme Wnt, régulateur important dans le développement du squelette. A l'aide de la technique ARN-Seq, nous confirmons que la PTH induit l'expression du gène *Lrp6* dans les ostéoblastes. Des études ChIP conventionelles confirment qu'une forme phosphorylée d'αNAC (αNAC-S99) interagit avec le promoteur de *Lrp6*. Enfin, des études utilisant les shRNA indiquent que l'inhibition d'αNAC provoque une réduction importante dans l'expression de *Lrp6*. Nos résultats indiquent qu'αNAC a pour function de contrôler l'expression de *Lrp6*. Dans nos recherches futures, nous visons à caractériser la nature moléculaire de l'interaction entre αNAC et le promoteur de *Lrp6*, et de déterminer son activité transcriptionnelle. Nous espérons mener des études sur des animaux transgéniques pour mieux comprendre les conséquences physiologiques de l'activité d'αNAC sur l'expression de *Lrp6* en réponse à la stimulation avec PTH.

Acknowledgments

I would first like to thank my supervisor, Dr. René St-Arnaud, for all of his support, encouragement, and mentorship throughout my time in his lab. Dr. St-Arnaud has a wonderful teaching style, where he has the ability to simultaneously provide insight on both the global picture as well as the critical details. I truly appreciated how he always made himself available whenever I needed to discuss challenges with my work, or how he delighted in sharing in new data results. Dr. St-Arnaud's mentorship made it possible for me to pursue my goals; both on a scientific and personal level, and for that I am truly grateful.

I would also like to thank Dr. Martin Pellicelli for his guidance and wonderful training at the bench. I feel truly fortunate to have had the opportunity to train under such a stellar scientist. His ability to help me overcome experimental challenges, his openness and availability for questions, and day-to-day support and encouragement have been invaluable during my time in the lab.

Thank you to my supervisory committee members, Dr. Pierre Moffatt and Dr. Robert Sladek, for their time and guidance throughout my project. I also wish to acknowledge the contributions made by the staff and scientists of the McGill University and Génome Québec Innovation Centre. My thanks and appreciation also goes to Hadla Hariri, for her additional contributions to my project. Her knowledge, encouragement, and friendship have been greatly appreciated as I reached the end of my Masters. A special thanks to all of my research colleagues past and present: Alice Arabian, Theresa Farhat, Toghrul Jafarov, Corine Martineau, Bahareh Hekmatnejad, Amanda Gerges, Rui Zhang, Laszlo Kupcsik, and Bachar Hamade.

My love and gratitude go to my wonderful parents who are exemplary models of the kind of parent I hope to be to my boys. Thank you to my sisters, Leslie and Emily, who have provided unconditional love and support to me from day one, no matter how far apart we may be. And finally, I am truly privileged to call Omar Ahmad my husband. Omar has always pushed me to chase after any dream that I have had, and I could not have achieved them without his love,

encouragement, and spectacular coffee. Thank you for being a truly remarkable husband, and incredible father to our boys. The biggest thank you goes to Elias, who has been with me on this scientific journey from the very beginning. He will always be my little infant scientist, who is now such a loving and kind little boy. Elias, you and your brother are by far my greatest achievement.

List of Figures

Introduction

Results

List of Tables

List of Abbreviations

6Bnz-cAMP	N6-benzoyladenosine cAMP
αMEM	α-Minimum essential medium
αNAC	Nascent polypeptide associated complex and coregulator α
µg	Microgram
µl	Microliter
AP-1	Activator protein 1
ATF4	Activating transcription factor 4
B2M	Beta-2-microglobulin
BMP	Bone morphogenetic protein
bp	Base pair
BSP	Bone Sialoprotein
cAMP	Cyclic adenosine monophosphate
CCD	Cleidocranial dysplasia
cDNA	Complementary deoxyribonucleic acid
c-JUN	Jun proto-oncogene
ChIP	Chromatin Immunoprecipitation
ChIP-seq	Chromatin Immunoprecipitation-sequencing
CK2	Casein kinase 2
Collα1	α_1(I) collagen
Ct	Cycle threshold
DBD	DNA-binding domain
Dkk1	Dickkopf
DMEM	Dulbeco's modified eagle's medium
ECL	Enhanced chemiluminescence
ECM	Extracellular matrix
EDTA	Ethylenediaminetetraacetic acid
EMSA	Electrophoretic mobility shift assay
FIAT	Factor inhibiting ATF4-mediated transcription
GPCR	G protein-coupled receptor
GSK3β	Glycogen synthase kinase 3β
HDAC	Histone deacetylase
HSC	Hematopoietic stem cells
ILK	Integrin-linked kinase

LEF1	Lymphoid enhancer-binding factor 1
Lrp6	Low-density lipoprotein-related protein 6
M-CSF	Macrophage colony stimulating factor
MSC	Mesenchymal stem cell
ng	Nanogram
nm	Nanometer
NCP	Nucleus/chromatin preparation
Ocn	Osteocalcin
OPG	Osteoprotegerin
OSE2	Osteoblast-specific element 2
OST-PTP	Osteotesticular protein tyrosine phosphatase
Osx	Osterix
PBS	Phosphate buffered saline
PCR	Polymerase chain reaction
PKA	Protein kinase A
PKAdn	Dominant-negative PKA
PTH	Parathyroid hormone
PTH1R	PTH/PTH-related peptide type 1 receptor
PTM	Post-translational modifications
PVDF	Polyvinylidene fluoride membrane
RANK	Receptor of activated Nuclear Factor-κB
RANKL	Receptor of activated Nuclear Factor-κB ligand
RIPA	Radio immunoprecipitation assay buffer
RT-PCR	Reverse transcriptase polymerase chain reaction
RT-qPCR	Real-time quantitative polymerase chain reaction
Runx2/Cbfa1	Runt-related transcription factor 2 / Core binding factor 1
shRNA	Small hairpin ribonucleic acid
siRNA	Small interfering ribonucleic acid
Sost	Sclerostin
SNS	Sympathetic nervous system
TBP	Tata binding protein
TBS	Tris-buffered saline
TBST	Tris-buffered saline Tween
TE	Tris-EDTA

TSS	Transcription start site
Wnt	Wingless integrated
Wt	Wild-type

I. Introduction

Overview

αNAC has been shown to regulate the transcriptional activity of the *Ocn* gene (Pellicelli et al. 2014; Akhouayri, Quélo, and St-Arnaud 2005). While *Ocn* remains our best-characterized gene target of αNAC, we hypothesized that there are additional bone-specific promoter targets of the αNAC transcriptional coregulator (Meury et al. 2010). The ChIP-seq analysis provided us with a number of potential gene targets across the mouse genome of which αNAC was predicted to bind. While we initially pursued 6 gene targets, we focused on characterizing αNAC's regulation of *Lrp6*. Quantitative ChIP assays have demonstrated that αNAC binds to the promoter of *Lrp6.* We investigated whether the PKA-mediated phosphorylated form of αNAC (αNAC-S99) is bound to the *Lrp6* promoter. We show that the S99 nuclear form of αNAC binds to the *Lrp6* promoter in osteoblasts with a relative promoter occupancy that is significantly greater than in vehicle-treated osteoblasts. Furthermore, we have identified a potential αNAC DNA binding-site within the promoter region of *Lrp6.*

1.1 Skeletal physiology

1.1.1 Overview of skeletal physiology

The skeleton serves a number of different functions in the body. It is a dynamic organ that provides the scaffolding and support system, which protects vital organs. The structural support of the skeleton allows for weight bearing activities; acting as a counter lever against muscle contractions, and a framework for complex movements. Contrary to previous thought, the skeleton is not an inert material, but is in fact an active and continually changing structure that undergoes numerous cycles of remodeling and new bone formation (Sommerfeldt and Rubin 2001)

In addition to providing structural and mechanical support, the skeleton acts as a mineral reservoir for mineral homeostasis. The mineralization of bone provides the body with a reserve

of calcium and phosphate in the form of hydroxyapatite crystals (Jensen, Gopalakrishnan, and Westendorf 2010). Interestingly, bone has the ability to respond to changes from both mechanical and metabolic demands of the body. The skeleton plays a unique role as an endocrine tissue, where it responds to changes in energy homeostasis through the coordination of a number different hormones, growth factors, and proteins. It is now evident that the skeletal system also plays an integral role in glucose metabolism (Karsenty and Ferron 2012; DiGirolamo, Clemens, and Kousteni 2012) .

The marrow space within bone provides a critically important environment for hematopoiesis to take place (Clarke 2008). Hematopoietic stem cells (HSC) occupy the marrow space, where they differentiate to form blood cellular components. Osteoclast bone cells are also derived from a HSC origin (Karsenty and Wagner 2002). Osteoclast cells, with respect to bone remodeling, have been shown to stimulate the mobilization of HSC out from the marrow space (Kollet et al. 2006; Boyce and Xing 2008). This finding shows the unique interplay between hematopoiesis and bone remodeling processes.

1.1.2 Skeletal histology: functions of main cell types

Bone is made up of three major cell types: (i) osteoblasts, (ii) osteocytes, and (iii) osteoclasts. Each of the different cell types play a role in skeletal longitudinal growth, bone formation, and bone remodeling. Osteoblast cells are primarily involved in new bone formation. Osteoblasts produce a non-calcified extracellular matrix (ECM) and subsequently regulate the mineralization process (Hartmann 2006).

Osteoblasts secrete a protein rich matrix that is mainly made up of type I collagen. Type I collagen fibers form a majority of the unmineralized bone matrix that makes up osteoid. In addition to the production of collagenous proteins, osteoblasts synthesize and secrete a number of non-collagenous proteins, such as osteocalcin (OCN), bone sialoprotein (BSP), osteopontin, and osteonectin. These non-collagenous proteins serve a number of different functions, such as

regulating bone cell activity, matrix mineralization, mineral deposition, and bone turnover (Clarke 2008).

Osteocytes are terminally differentiated from mature osteoblast cells. As the matrix mineralizes some osteoblasts can become embedded within the calcified matrix, where they undergo differentiation to become osteocytes. As osteoblasts mature, some are designated for apoptosis or become bone-lining cells; however, the remainder differentiate to become osteocytes (Knothe Tate et al. 2004). Osteocytes develop intricate networks as they become embedded within the matrix, where their cytoplasmic projections branch out to reach bone surface lining cells. These cytoplasmic projections, called filipodia, extend from the lacunae where they reside to within the canaliculi. The extensive communication networks are thought to direct sites for bone formation and remodeling. For example, osteocyte apoptosis is thought to be a contributing regulator of bone remodeling. However, the main function of osteocytes has been shown to be its role as transducers of biomechanical forces (Knothe Tate et al. 2004; Clarke 2008). Osteocytes are thought to signal the recruitment of osteoclasts to sites undergoing mechanical stress so that bone remodeling can take place (Boyce and Xing 2008). Additionally, modulation of fluid within the canaliculi, as well as the flow of minerals is thought to be in response to the bending and stretching of bone.

Osteoclasts are the third major type of bone cell, and are mainly involved in the resorption of mineralized bone. Unlike osteoblasts and osteocytes, which differentiate from mesenchymal stem cells (MSC), osteoclasts are terminally differentiated from monocyte-macrophages of HSC lineage (Sommerfeldt and Rubin 2001). Commitment and differentiation of osteoclasts from osteoclast precursors requires the cytokines macrophage-colony stimulating factor (M-CSF), and receptor activated Nuclear Factor-κB ligand (RANKL) (Raggatt and Partridge 2010). Osteoclasts have a unique morphology that distinguishes them from other bone cells. They are multi-nucleated cells, possess an apical membrane, a number of lysosomal enzymes, express tartrate-resistant acid phosphatase (TRAP), and the calcitonin receptor

(Raggatt and Partridge 2010). Osteoclast cells become polarized when they bind to the mineralized matrix, allowing them to produce their distinct apical membrane. There they secrete H^+ ions, exocytose cathepsin K, and other acidic enzymes in order to digest the bone matrix. Osteoclast formation is inhibited by osteoprotegerin (OPG), another TNF-superfamily cytokine receptor. OPG is an osteoblast-secreted protein, which acts as a soluble decoy receptor binding to RANKL. In the presence of OPG, RANKL becomes bound to OPG, thus preventing it from binding to RANK and inhibiting mature osteoclast formation. RANKL- stimulated osteoclastogenesis is regulated by the ratio of RANKL and OPG produced by osteoblast cells (Boyce and Xing 2008; Clarke 2008).

1.1.3 Bone modeling and remodeling

Throughout life bone is constantly undergoing continuous cycles of bone growth, modeling, and remodeling. These cycles are critical for the maintenance of skeletal health, as well as maintaining mineral homeostasis. Both osteoblasts and osteoclasts are involved in bone modeling and remodeling. However, a key distinction between the two processes is that modeling is coordinated by the independent actions of bone cells, while remodeling is regulated by the interplay and coupling action of osteoblasts and osteoclasts (**Figure 1**) (Andersen et al. 2009).

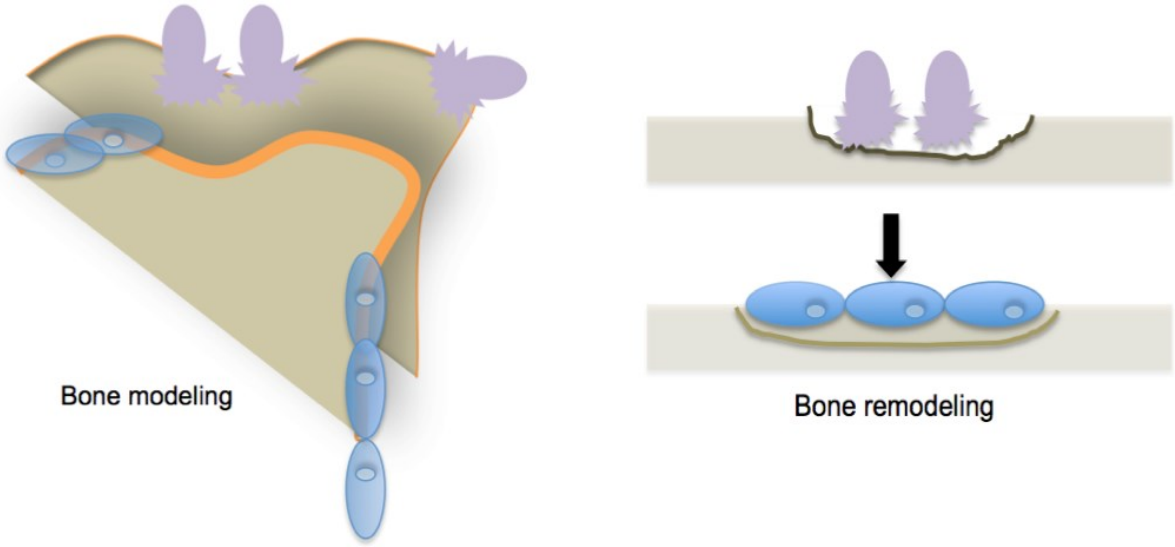

Figure 1. Bone modeling and remodeling mechanisms.

During bone modeling (left panel) the activity of bone cells is uncoupled and occurs at different sites. Therefore, new bone formation can occur at a site independent of where bone resorption is being carried out. In contrast, during bone remodeling (right panel) the coordination of osteoblast (blue cells) and osteoclast (purple cells) activity is intricately coupled. Remodeling occurs at the same bone site and is carried out sequentially. Bone remodeling is required for proper bone health to ensure tissue turnover and maintenance of normal bone mass. Figure modified from (Teti 2011)

Modeling is responsible for large changes in bone shape (Baek and Kim 2010). Longitudinal growth is attributed to endochondral bone formation, and the elongation at the epiphysis of long bones, while radial growth occurs through continued bone modeling. Appositional growth occurs on the periosteal surface, where bones continue to increase in diameter throughout life (Clarke 2008; Baek and Kim 2010). Additionally, modeling responds to mechanical loading, tailoring the appropriate shape of the bone in response to biomechanical stress and growth.

Bone remodeling does not produce large changes in bone shape, but is responsible for maintaining and repairing the skeletal structure. Bone remodeling is initiated in response to various stimuli. Site directed remodeling is not fully understood, however some of the contributing factors are microfractures of the bone due to normal wear, biomechanical stress due to changes in body shape or physical activity, normal growth, and weight gain (Boyce and Xing 2008).

1.1.4 Hormonal regulation of bone modeling and remodeling

Parathyroid hormone (PTH) has a dynamic role in maintaining mineral homeostasis. PTH regulates calcium and phosphate levels by stimulating the mobilization of calcium in response to changes in circulating extracellular calcium levels sensed by the calcium sensing receptor (**Figure 2**). In order to increase circulating calcium levels, osteoclasts increase bone resorption activity, which mobilizes calcium and phosphate from bone into the blood (Raggatt and Partridge 2010). PTH also mobilizes calcium through reabsorption in the kidney as well as through vitamin D synthesis. PTH regulates the enzyme 1α-hydroxylase, which converts vitamin D to its active form, $1,25(OH)_2D$ (DiGirolamo, Clemens, and Kousteni 2012). Active vitamin D increases intestinal reabsorption of calcium and phosphate. Additionally, PTH regulates phosphate by controlling the amount of phosphate reabsorbed in the kidney. Sodium-phosphate co-transporters are downregulated by PTH, leading to phosphate reabsorption in the distal convoluted tubule of the kidney. Fibroblast growth factor 23 (FGF23) acts as a part of a negative

regulatory feedback loop to inhibit PTH activity. FGF23 is made in bone by osteocytes, and regulates the excretion of phosphate from the kidney by inhibiting PTH at the level of the parathyroid gland, and 1,25$(OH)_2$D in the kidney (Shimada and Kakitani 2004; DiGirolamo, Clemens, and Kousteni 2012).

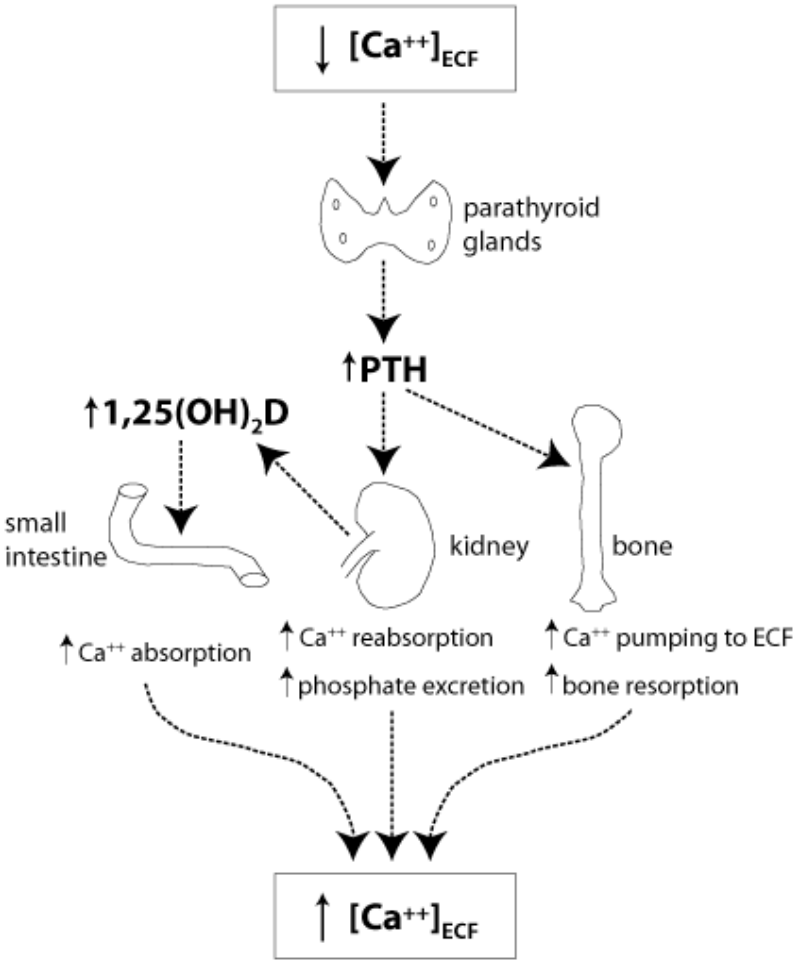

Figure 2. The role of PTH in calcium and phosphate mineral homeostasis.

PTH is secreted by the parathyroid gland in response to a decrease in serum calcium levels. PTH targets bone and the kidney to regulate calcium and phosphate. PTH secretion increases osteoclastic activity, which releases calcium and phosphate from the bone. The conversion of vitamin D to its active form leads to the regulation of calcium and phosphate levels via the kidney and small intestine.

1.1.4.1 Intermittent exposure to PTH stimulates bone formation

PTH can either exert an anabolic or catabolic effect depending on whether it is expressed intermittently or continuously (Jilka 2007). The previous depiction of PTH activity highlights its catabolic effect, in which calcium and phosphate are leached from the bone into circulation by activating key bone resorption factors. However, the dual nature of PTH is such that intermittent exposure has been shown to have a formidable anabolic effect on bone formation (Tam et al.1982; Jilka 2007).

The human form of PTH is 84 amino acids long, while its therapeutic analogue, teriparatide, is a truncated form of PTH consisting of amino acids 1-34 (Hodsman et al. 2005). Teriparatide acts as a remodeling inhibitor, thus improving patients bone density and bone porosity. Teriparatide is currently the only approved anabolic treatment for osteoporosis. This anabolic therapeutic offers numerous advantages for patients with osteoporosis, such as increasing bone formation, and preventing the rate of fracture (Hodsman et al. 2005). Conversely, there are a number of factors that make teriparatide an undesirable therapeutic. Disadvantages for administration of teriparatide include the high cost of the drug, the subcutaneous injection delivery route, as well as the increased risk of osteosarcoma that was seen in animal models (Vondracek 2010). Since the risk of osteosarcoma due to teriparatide treatment has not yet been fully delineated in humans, patients can only undergo teriparatide therapy for up to two years. PTH and its analogues have proven to be powerful agents in rebuilding bone health; therefore, it is of critical importance to identify alternative targets within the PTH signaling pathway as potential anabolic therapeutics.

1.1.5 Diseases related to bone modeling and remodeling: osteoporosis and osteopetrosis

It is critical that the balance and rate of bone turnover are properly maintained. Disruption of the equilibrium between bone formation and bone turnover is evident in several diseases such

as osteoporosis and osteopetrosis. Osteoporosis is in part due to increased osteoclastic activity, where bone resorption occurs at a greater rate than osteoblast-mediated bone formation. This leads to low bone mass, and more porous brittle bones. This leaves osteoporotic bones much more susceptible to fracture. Conversely, osteopetrosis is attributed to increased bone formation and impaired osteoclastic activity, where bone formation occurs at a much greater rate than bone resorption. Patients with osteopetrosis have increased bone mass, and loss of the bone marrow cavity (Karsenty and Wagner 2002).

1.1.6 Osteocalcin: An osteoblast-specific protein that regulates glucose metabolism

As previously mentioned, bone plays a critical role in energy and glucose metabolism. It has recently been shown that OCN, an osteoblast-specific protein and late-marker of osteoblast differentiation, is regulated by insulin. Mice that lack OCN display a phenotype similar to diabetes mellitus type 2 (Lee et al. 2007). OCN contains three glutamic acids that remain susceptible to carboxylation. When OCN remains undercarboxylated it is in its active form, and it acts as a hormone regulating insulin expression. In contrast, by carboxylating OCN the protein OST-PTP acts as a negative regulator of OCN metabolic activity. Insulin modulates the expression and availability of undercarboxylated OCN by suppressing the production of OPG. A lack of OPG, an osteoblast-derived decoy receptor, prevents the inhibition of osteoclastogenic activity. Increased osteoclast activity leads to enhanced bone resorption, which lowers the pH and increases the conversion and availability of undercarboxylated OCN from carboxylated OCN (DiGirolamo, Clemens, and Kousteni 2012). Undercarboxylated OCN signals to β-cells to increase β-cell proliferation and insulin production. Leptin, a hormone secreted by adipocytes, acts as a suppressor within this feedback loop. Leptin inhibits OCN activity via activation of the sympathetic nervous system (SNS) (Takeda et al. 2002). The activation of the SNS occurs through the ventral hypothalamus, which stimulates the release of norepinephrine and activates the β2 adrenergic receptor on osteoblast cells subsequently inhibits OCN activity of insulin

secretion (Hinoi et al. 2008; Takeda et al. 2002; Karsenty and Ferron 2012). The interplay between OCN-mediated glucose metabolism and bone remodeling, demonstrates the critical role that bone cells play in regulating energy homeostasis.

1.2. Skeletal development

1.2.1 Differentiation of skeletal tissue from mesenchymal stem cells.

The skeleton consists of two different types of tissue: cartilage and bone. Two of the 3 major cell types, chondrocytes and osteoblasts, which produce cartilage and bone, differentiate from MSCs (**Figure 3**). These multipotent MSCs, which are derived from the mesoderm, have the potential to differentiate into a number of key cell types: chondrocytes, osteoblasts, myocytes, and adipocytes to name a few (**Figure 3**) (Pittenger et al. 1999).

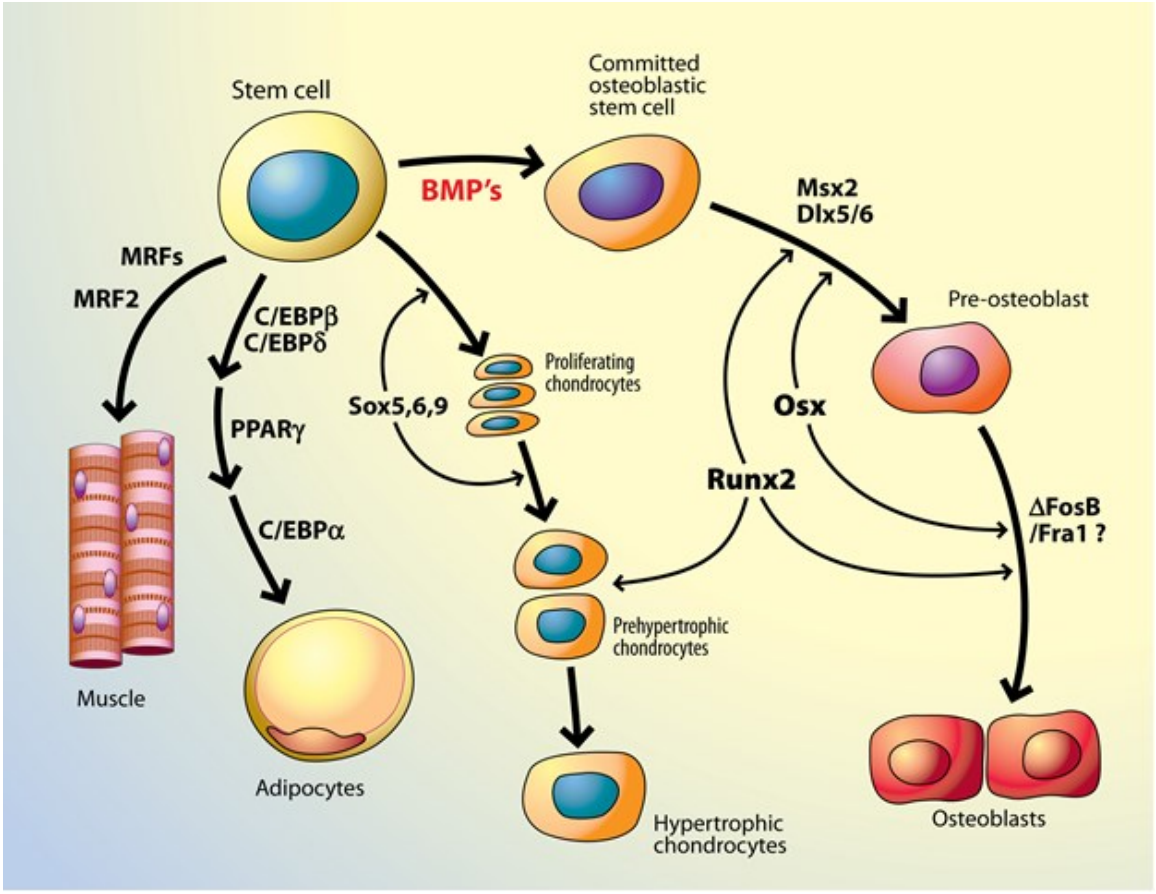

Figure 3. Multipotent MSCs give rise to a number of cell lineages critical in skeletal formation.

Skeletal tissue is produced from mesenchymal stem cells. Transcription factors contribute to controlling the commitment and differentiation from osteoprogenitor cells to specific lineages. Pictured above are the different cell types that differentiate from MSCs to become different mesodermal lineages, and some of the transcription factors that regulate their commitment and differentiation.

MSCs differentiate to become chondrocytes, which in turn further differentiate to become a number of different kinds of cartilaginous tissue. Chondrocytes are the first skeletogenic cell type to appear during early development (Karsenty, Kronenberg, and Settembre 2009). Skeletal development that begins with chondrogenesis, forming an anlagen of future bones to undergo mineralization, is termed endochondral ossification (Sommerfeldt and Rubin 2001). In addition to the role cartilage plays in osteogenesis, cartilage tissue provides joint flexibility, absorbs shock from weight-bearing activities, and reduces friction between joints. Chondrocytes are also largely responsible for the longitudinal growth of the axial skeleton (Karsenty, Kronenberg, and Settembre 2009).

Lineage commitment of osteoblasts from MSCs is in part coordinated by the canonical wingless integrated (Wnt) signaling pathway. The importance of Wnt signaling in osteoblast commitment is first evident in its repression of adipocyte and chondrocyte differentiation from MSCs in favor of osteoblast progenitor cells (**Figure 4**). Just as Wnt factors stimulate osteoblast differentiation, and promote increased osteoblast proliferation, there exists a negative feedback loop where osteoblasts regulate the expression of Wnt (Baron and Rawadi 2007). Mature osteoblasts produce factors such as Dickkopf (Dkk1) and sclerostin (Sost), which act to inhibit the Wnt signaling pathway (Morvan et al. 2006).

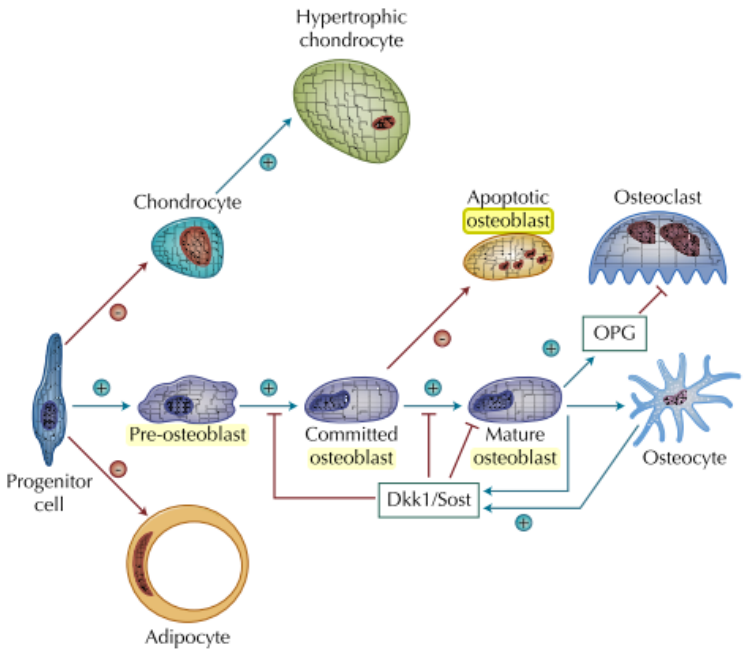

Figure 4. Osteoblast lineage commitment through the regulation of Wnt signaling.

Wnt signaling regulates the commitment to osteoblast lineage from osteoprogenitor cells. Wnt signaling promotes osteoblast differentiation through the suppression of adipocyte and chondrocyte lineages. Wnt antagonists, Dkk1 and Sost, act to suppress osteoblast differentiation. The production of Wnt antagonists functions as a negative feedback loop where osteoblasts regulate the expression of Wnt. Figure reproduced from (Baron and Rawadi 2007).

1.2.2 The canonical Wnt signaling pathway and bone development

Canonical Wnt signaling is a well-characterized critical pathway regulating bone homeostasis. Wnt signaling has been shown to control the commitment of MSCs to osteoblastic lineage, as well as regulating additional factors controlling bone mass (Baron and Rawadi 2007). Genetic studies have delineated the role of Wnt signaling such that a gain-of-function mutation leads to increased bone mass, while loss-of-function leads to decreased bone mass (Baron and Kneissel 2013). Canonical Wnt signaling is activated via binding of Wnt activators to the complex formed by the G protein-coupled receptor (GPCR) frizzled to either low-density lipoprotein-related protein 5 (LRP5) or LRP6, which then activate a number of downstream targets. Formation of this complex results in the inactivation of β-catenin degradation. β-catenin accumulates in the cytosol and translocates to the nucleus where it activates gene transcription, rather than designation for proteasomal degradation (Baron and Kneissel 2013). Recent work on canonical Wnt signaling supports the idea of activation or inhibition of factors within the pathway though the crosstalk from other pathways, such as PTH signaling. One example of Wnt-PTH crosstalk is PTH-induced suppression of *Sost,* a negative regulator of Wnt signaling (T. Bellido et al. 2005).

One of the aims for this thesis is to examine the control of the expression of *Lrp6*, an essential Wnt signaling protein, via PTH-induced αNAC-mediated transcriptional activation. LRP6 has largely been thought to play a role mainly in the regulation of bone mass by acting as a co-receptor for the activation of the canonical Wnt signaling pathway and the stabilization of β-catenin (Baron and Rawadi 2007). Phenotypic characterization of LRP6 has been carried out through loss and gain-of-function studies, which exemplify the low and high bone mass phenotype respectively. Following the binding of PTH to the receptor, the extracellular domain of LRP6 complexes with PTH/PTH-related peptide type 1 receptor (PTH1R) forming a ternary complex (PTH/PTH1R/LRP6) (Wan et al. 2008). Protein kinase A (PKA) then phosphorylates LRP6 on its intracellular domain, which acts to stabilize β-catenin expression, a critical mediator

for osteoblast bone formation via Wnt signaling or the PTH pathway (Wan et al. 2008). Knock down of LRP6 by siRNA leads to an accumulation of β-catenin in the cytosol, as well as a reduction of osteoblast-mediated bone formation markers. In LRP5-deficient mouse models, PTH can still stimulate new bone formation, indicating different roles for LRP5/LRP6 in bone formation (Iwaniec et al. 2007; Wan et al. 2008). This suggests that LRP6 plays a critical role in the PTH signaling pathway and proliferation of osteoprogenitors. An area still under investigation is how the binding of LRP5 or LRP6 to the (PTH/PTH1R/LRP6) ternary complex, or to different Wnt receptors, may alter the signaling output. Additionally, ligands outside of Wnt signaling that bind with LRP5/6 are not yet well understood. To further understand the effect of these proteins on bone development it is critical to investigate how such cofactors might modulate the role or activity of LRP5/6 (Hartmann 2006).

1.2.3 Ossification

Skeletal development begins as early as embryonic day 10.5, where cells from the mesenchyme begin to condense and differentiate into cells necessary to form a template of the future skeleton (Karsenty, Kronenberg, and Settembre 2009). Skeletal development continues through two different ossification processes (i) endochondral ossification and (ii) intramembranous ossification (**Figure 5**). Endochondral ossification begins in early development with the formation of a cartilage precast preceding the formation of mineralized bone. Chondrocytes located in the middle of the skeletal precast begin to produce type II ECM, which is rich in proteoglycans. The formation of prehypertrophic chondrocytes is preceded by the rapid proliferation of chondrocytes and ensuing arrest of the cell cycle. The prehypertrophic chondrocytes continue to produce type II collagen matrix, and the transition to the production of type X collagen signifies their differentiation into hypertrophic chondrocytes (Karsenty, Kronenberg, and Settembre 2009).

Apoptosis of hypertrophic chondrocytes accompanies vascular innervation of the developing bone, which introduces osteoblast precursor cells deep at the center of the cartilage precast. Here the osteoblast precursors form a primary ossification center in the diaphysis of long bones. At this time the perichondrium differentiates into the periosteum with osteoprogenitor cells forming the bone collar. The bone collar will eventually become cortical bone, a critical site for appositional growth (Clarke 2008). Osteoblasts produce a protein-rich ECM made up of type I collagen, which is laid down on top of the remnants of the type X collagen matrix secreted by hypertrophic chondrocytes. This spongy like bone forms the primary spongiosa, which will become trabecular bone (Karsenty, Kronenberg, and Settembre 2009). Proliferating chondrocytes, hypertrophic chondrocytes, and ECM form the cartilage layer that makes up the growth plate, which is located between the diaphysis and epiphysis of long bones. The epiphyseal growth plate is mainly responsible for longitudinal growth. The site for secondary ossification is located in the epiphysis of long bones, which becomes active after birth and remains active until adult height is reached during adolescence.

Bone tissue can develop into four different kinds of bone: long bones, short bones, flat bones, and irregular bones. The ossification process, which will be further discussed, varies depending on the bone type (Clarke 2008). All four categories of bone are made up of cortical and trabecular bone. The ratio of cortical to trabecular bone depends on the bone type, but overall a majority of the adult skeleton consists of cortical bone. In long bones cortical bone tissue surrounds the marrow space, and can be found in the diaphysis. In contrast to the dense nature of cortical bone, the metaphysis and epiphysis contain trabecular bone, which creates a 3-dimensional honeycomb-like network inside the marrow space. In early life bone tissue is constantly undergoing longitudinal and radial growth. However, once adult height is reached bone continues to respond to changes in the environment and undergo modeling and remodeling.

The process of intramembranous ossification occurs in bones of the skull, maxilla, mandible, and lateral portions of the clavicle. Intramembranous ossification does not require a cartilage intermediary for bone mineralization to occur. Instead, bone formation occurs within membranous tissue, eventually becoming mineralized bone. Many of the bones that undergo intramembranous ossification are of neural crest origin. As the neural crest closes mesenchymal condensations begin to form, signaling the induction of osteogenesis. Condensations form by an increasing number of cells migrating towards the center of condensation, rather than increased proliferation or cell apoptosis (Franz-Odendaal 2011). Osteoblast cells begin to differentiate from osteo-chondroprogenitor cells, and pattern the membranous skeletal template that began to form early in development (Franz-Odendaal 2011). Finally, osteoblast cells begin to secrete a protein-rich collagenous matrix forming the osteoid. The gelatinous matrix of the osteoid is eventually replaced with a calcified bone matrix, where mature osteoblasts differentiate into osteocytes and become embedded in the mineralized bone. Intramembranous bone formation is in part regulated by a number of different paracrine signaling molecules, such as Ihh, Wnt, BMP, and FGF (Franz-Odendaal 2011). In addition to these signaling molecules there are number of transcription factors that exert transcriptional regulation on cell differentiation and osteogenesis.

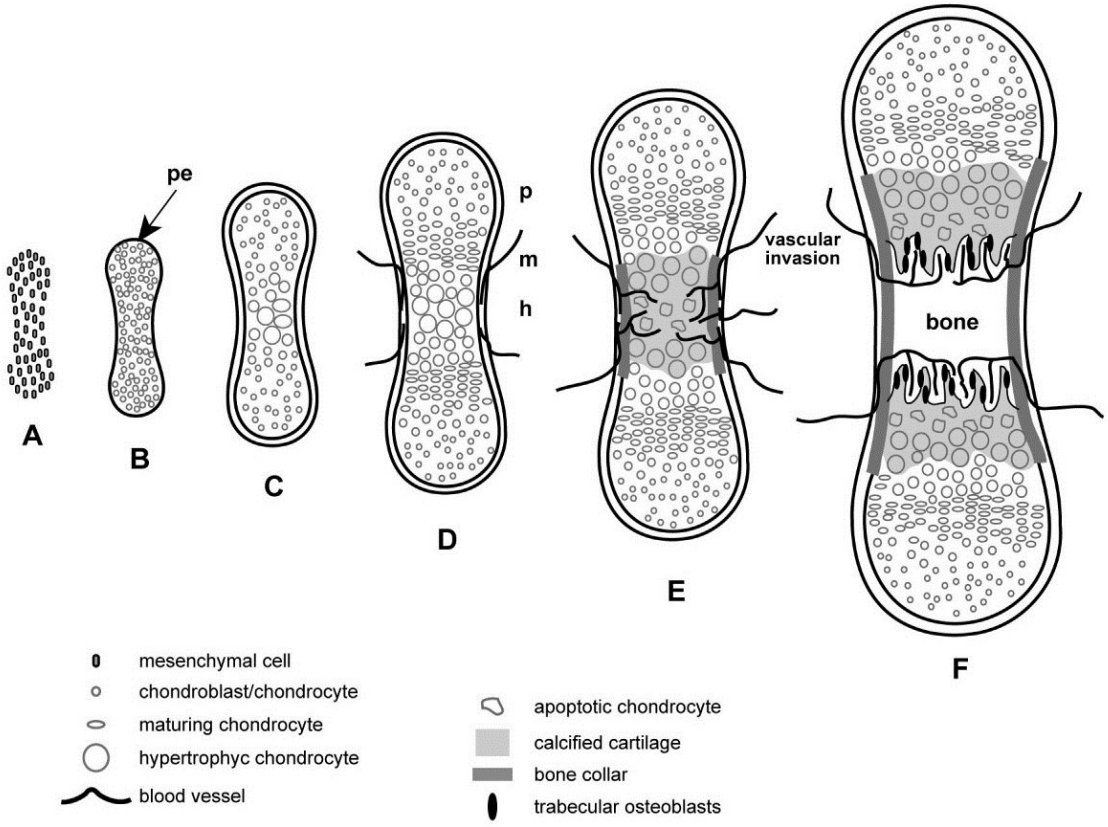

Figure 5. Schematic of endochondral ossification.

Skeletal formation and mineralization is carried out by one of two processes: (a) intramembranous ossification and (b) endochondral ossification. In intramembranous ossification skeletal formation is carried out without a cartilage precast. During intramembranous ossification the condensed mesenchyme differentiates to produce osteoblast cells, which secrete osteoid that subsequently mineralizes to form compact bone. Endochondral ossification (pictured above) occurs with a cartilage precast preceding bone mineralization. Chondrocytes form within the condensed mesenchyme. As they proliferate and grow they form hypertrophic chondrocytes. As hypertrophic chondrocytes apoptose vascular innervation occurs. Preosteoblasts begin to differentiate into osteoblasts, and secrete osteoid on top of the cartilage scaffolding. Osteoclasts increase resorption activity in concert with matrix mineralization, which creates the hollow architecture of trabecular bone.

1.2.4 Genetic regulation of osteoblastogenesis

Osteoblasts differentiate from MSCs, and the commitment and differentiation of these cells is tightly regulated by a number of master transcriptional regulators. Transcription factors that promote osteoblastogenesis are tightly regulated by other regulatory proteins, transcription factors, growth factors, hormones, and by mechanical forces (Marie 2008). Our understanding of osteoblast transcriptional regulation has largely been elucidated by a number of molecular and genetic studies using mouse models involving genetic manipulation of specific transcription factors (Marie 2008). We will briefly describe the role and regulation of two master transcription factors in osteoblastogenesis: runt-related transcription factor 2 (Runx2) and Osterix (Osx).

1.2.4.1 Transcription factors regulating osteoblastogenesis

Runx2 is considered the principal transcription factor that commits a MSC to the osteo-chondroprogenitor lineage (Ducy et al. 1997). These cells have the capacity to further differentiate into either osteoblasts or chondrocytes. The expression of Runx2 is critical in early skeletal development, and continues to be expressed during postnatal development as well (Ducy et al. 1997; Marie 2008). In *Runx2/Cbfa1*-deficient mice both endochondral and intramembranous ossification is inhibited. The loss of proper ossification further underscores Runx2 as a master regulator for both chondrocyte and osteoblast differentiation (Komori et al. 1997). The critical function of Runx2 in bone development is evident in human diseases where there is a loss of function in *Runx2* expression. Mice that express *Runx2/Cbfa1* in only one allele, $Cbfa1^{+/-}$, exhibit defects in bones that undergo intramembranous ossification (Karsenty and Wagner 2002). Cleidocranial dysplasia (CCD) is the human form of this disease; an autosomal dominant disorder whereby haploinsufficiency in CCD patients results in a series of skeletal abnormalities due to mutations in the RUNX2 protein (Mundlos et al. 1997; Jensen, Gopalakrishnan, and Westendorf 2010). $Cbfa1^{+/-}$ mice are phenotypically similar to CCD, and therefore are characterized by hypoplasia of the clavicles and nasal bone, and arrested ossification along the skull sutures (Komori et al. 1997).

Positive regulation of *Runx2* is carried out by a number of different coactivators; the most prevalent coactivator being CBFβ1 (Karsenty, Kronenberg, and Settembre 2009). Additionally, *Runx2* is regulated by a series of histone acetyltransferases, which modifies the protein-protein interaction of RUNX2, and alters protein stability (Jensen, Gopalakrishnan, and Westendorf 2010). PTH is also a key regulator of Runx2 activation; its phosphorylation confers an anti-apoptotic effect on osteoblast cells (Bellido et al. 2003). PTH attenuates this apoptotic effect by inhibiting factors that designate RUNX2 for degradation. The prolonged overexpression of RUNX2 induced by PTH activity thereby promotes bone anabolism (Bellido et al. 2003). *Runx2* is negatively regulated by histone deacetylases (HDACs), which act to inhibit osteoblast differentiation. In addition to the HDACs, Sox9, a critical chondrogenic transcription factor, inhibits the transcriptional activity of Runx2; while Sox8 inhibits terminal differentiation of osteoblasts by acting as a direct negative regulator of *Runx2* promoter activity (Schmidt et al. 2005).

RUNX2 activates osteogenic gene transcription by recognizing and binding to the osteoblast-specific element (OSE2) or Runx regulatory element (Ducy and Karsenty 1995). The promoter region of all osteoblast cells contain the OSE2 consensus sequence PuACCPuCA (Komori et al. 1997). The binding of this consensus sequence has been used to characterize the genome-wide binding sites of RUNX2. This study offers insight into the role of RUNX2 in its regulation of cell differentiation, proliferation, and its function with respect to cancer (Håkelien, Bryne, and Harstad 2014).

Osterix (Osx), a novel zinc finger-containing transcription factor, is necessary for mature osteoblast differentiation. In *Osx*-deficient mice mature osteoblast formation, and bone formation cannot occur (Nakashima et al. 2002). Homozygous mutants exhibit normal cartilage formation, but completely lack proper formation and mineralization of the skeleton (Nakashima et al. 2002). This is evident in bones that undergo endochondral and intramembranous ossification. The arresting of osteoblast differentiation and ossification processes occurs at a

later time point than in *Runx2*-deficient mice. Runx2 is expressed throughout osteoblast differentiation and maturation. *Runx2/Cbfa1* null mice do not express Osx, however *Osx*-deficient mice do express *Runx2.* This key finding indicates that Osx functions downstream of Runx2 (Nakashima et al. 2002).

Osx-null mice exhibit a lack of differentiated osteoblasts. Disruption of mature osteoblast differentiation is supported by the lack of expression of mature osteoblast markers, such as OCN, BSP, and osteonectin. Osx has also been shown to regulate osteoblast proliferation, via inhibition of the Wnt signaling pathway (Zhang et al. 2008). Regulation of osteoblast proliferation by Osx adds an additional level of control to ensure the proper rate of bone formation (Zhang 2010). Osx regulates the expression of the Wnt antagonist Dkk1, by binding to its promoter and activating its transcription. Dkk1 works to inhibit preosteoblasts from differentiating into mature osteoblasts (**Figure 4**). Additionally, Osx has been shown to disrupt the binding of the TCF/LEF to DNA (Zhang et al. 2008). TCF/LEF plays a critical role in canonical Wnt signaling where it regulates gene transcription of target Wnt genes (Baron and Rawadi 2007).

1.3 αNAC: A coregulatory protein in bone

The nascent polypeptide associated complex and coregulator alpha (αNAC) is a bone-enriched transcriptional coregulator that is ubiquitously expressed postnatally. αNAC expression is seen mainly in bone during development (Moreau et al. 1998). Coregulatory proteins help to regulate transcription factors that bind to DNA and either upregulate or inhibit gene expression. The transcription factors that coordinate osteoblast differentiation and bone formation are further regulated by a number of coregulatory proteins. Mutations in αNAC are embryonic lethal suggesting that it plays a critical role in development (Meury et al. 2010). NAC is best understood for its role in the cytoplasm (Kramer et al. 2009; Wiedmann et al. 1994), where αNAC and βNAC form a heterodimeric protein that plays a role in proteostasis. NAC is thought to mainly function as a ribosome-associated protein chaperone where it stabilizes short newly

synthesized polypeptide chains. Under suitable conditions, αNAC translocates from the cytoplasm to the nucleus, where it acts as a transcriptional coregulator (Quélo et al. 2004a, Jafarov, Alexander, and St-Arnaud 2012; Hekmatnejad et al. 2014).

The role of αNAC as a transcriptional coactivator is exhibited by its interaction with the basal transcriptional machinery (Yotov, Moreau, and St-Arnaud 1998). αNAC can bind DNA on its own, but cannot independently initiate transcription (Akhouayri, Quélo, and St-Arnaud 2005). αNAC can however potentiate the activity of GAL4/VP-16, a chimeric transcriptional activator, and enhance activated transcription (Yotov, Moreau, and St-Arnaud 1998; Sadowski et al. 1988). Additionally, affinity chromatography demonstrated that αNAC has a strong protein-protein interaction with the TATA binding protein (TBP). αNAC exhibits coactivating properties through this protein-protein interaction with TBP (Yotov, Moreau, and St-Arnaud 1998).

1.3.1 αNAC and its role in the nucleus

αNAC has a distinct role in the nucleus that is separate from its role in proteostasis as a heterodimeric protein. Following translocation from the cytosol to the nucleus, αNAC works as an osteoblast-specific AP-1 coactivator, where it potentiates the activity of the c-Jun proto-oncogene (c-JUN) homodimer at the *Ocn* promoter by interacting with the basal transcription factor TBP (**Figure 6**) (Akhouayri, Quélo, and St-Arnaud 2005; Moreau et al. 1998). Inhibition of endogenous αNAC through siRNA, diminishes *Ocn* promoter activity in osteoblast cells (Akhouayri, Quélo, and St-Arnaud 2005). Taken together, αNAC has a critical role in regulating bone-specific gene transcription.

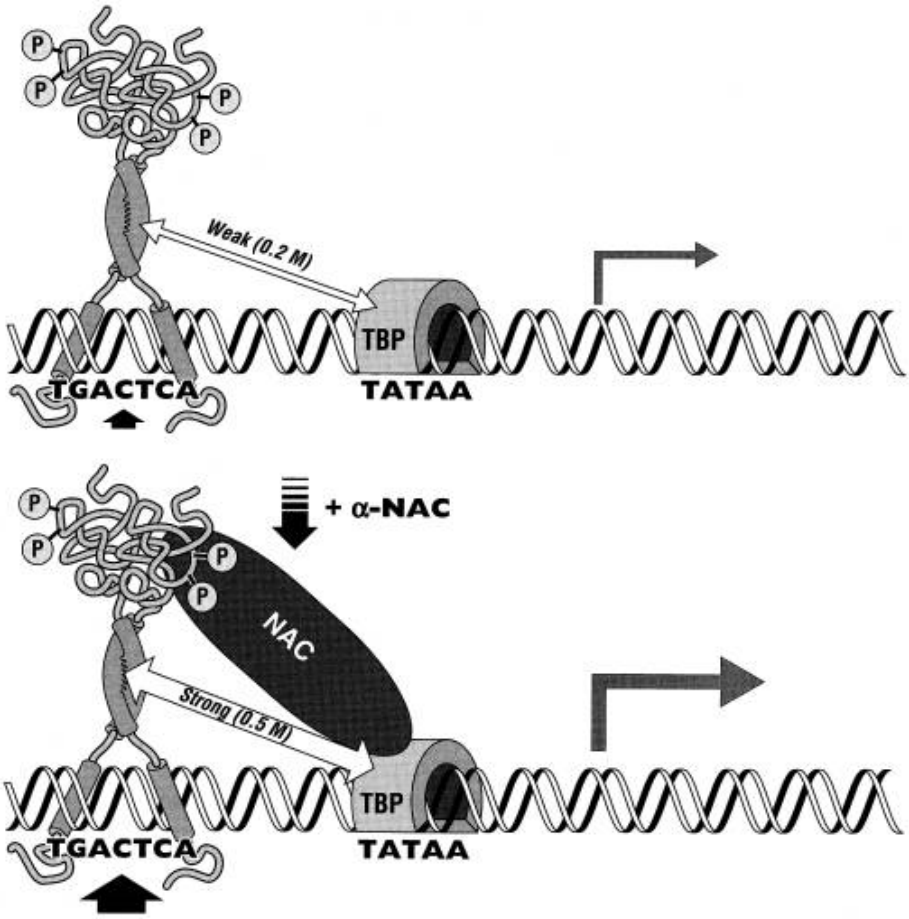

Figure 6. αNAC functions as a transcriptional coactivator.

αNAC creates a protein bridge with part of the basal transcriptional machinery, the TATA binding protein. αNAC also forms a protein-protein interaction with both the phosphorylated and unphosphoryated form of the c-JUN homodimer. c-JUN alone binds the AP-1 binding site, however this is a weak interaction with the TBP. The formation of the c-JUN/ αNAC /TBP ternary complex potentiates the expression of c-JUN-dependent *Ocn* gene transcription. Figure reproduced from (Moreau et al. 1998).

There is evidence that nuclear αNAC can have both coactivator and corepressor functions, and that these functions are in part mediated by interactions with other nuclear proteins. In cells of osteoblastic lineage, αNAC binds to the *Myogenin* promoter where it acts as a corepressor through its interaction with HDAC1 and HDAC3; whereas in myoblasts, αNAC acts as a corepressor at the *Ocn* promoter (Jafarov, Alexander, and St-Arnaud 2012). These initial findings led to the revision of the role of αNAC as a docking platform for the recruitment of transcriptional activators or repressors. Additionally, when αNAC undergoes post-translational modifications (PTM), such as simultaneous phosphorylation and SUMOylation, it is then capable of recruiting HDAC2 where it represses the ATF4-mediated transcriptional activation of *Ocn* (**Figure 7**) (Hekmatnejad et al. 2014).

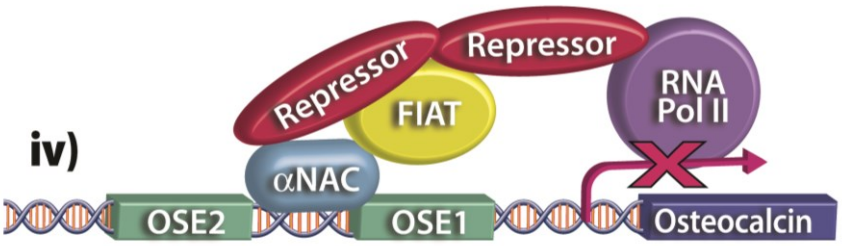

Figure 7. αNAC functions as a transcriptional corepressor.

αNAC or FIAT recruits repressors such as HDAC to inhibit the transcriptional activation of *Ocn*. αNAC can act as a transcriptional coactivator or corepressor. Following the post-translational modification of SUMOylation, and in coordination with FIAT, αNAC acts a corepressor where it enhances FIATs inhibitory effect on ATF4-mediated *Ocn* gene transcription. Figure reproduced from (St-Arnaud and Hekmatnejad 2011).

1.3.2 Phosphorylation by effector kinases leads to the nuclear localization of αNAC

αNAC undergoes post-translational modifications by different effector kinases at a number of specific residues (**Figure 8**). When αNAC is phosphorylated at residue serine 43 by integrin-linked kinase (ILK) it promotes the translocation of αNAC from the cytosol into the nucleus. Phosphorylation of αNAC by ILK is also required for the potentiation of c-JUN mediated responses (Quélo et al. 2004a). Phosphorylation of αNAC at several phosphoacceptor sites at its amino terminus by casein kinase 2 (CK2) controls the nuclear export of αNAC (Quélo et al. 2005). Phosphorylation of αNAC at position threonine 159 by glycogen synthase kinase 3β (GSK3β) designates αNAC for proteasomal degradation. Inhibition of GSK3β prevents αNAC from being directed for proteasomal degradation, and thereby promotes the nuclear translocation of αNAC (Quélo et al. 2004b). In addition to the kinases listed above, there are yet other kinases that regulate the shuttling of αNAC from the cytosol to the nucleus, where αNAC can differentially act as positive or negative regulator of gene transcription. There is an ongoing effort to delineate the role of these additional kinases and their affect in regulating αNAC.

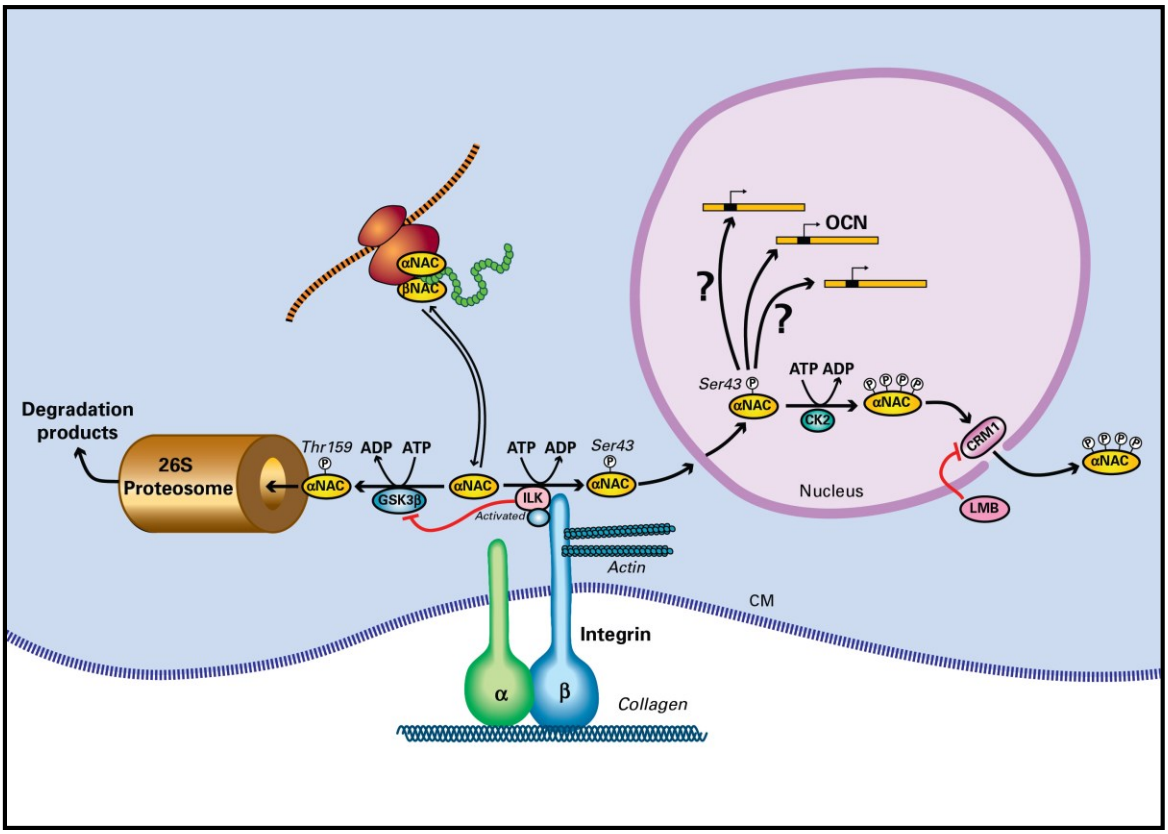

Figure 8. Phosphorylation of αNAC by effector kinases.

ILK phosphorylates αNAC and designates it for translocation from the cytosol into the nucleus where it acts as a transcriptional coregulator. CK2 promotes the nuclear export of αNAC. GSK3β directs αNAC to the proteasome for degradation.

1.3.3 The role of αNAC in a PTH-initiated signaling cascade mediated by PKA

Following activation by PTH signaling, αNAC acts as a substrate of PKA where it phosphorylates αNAC at serine 99 (αNAC-S99) (Pellicelli et al. 2014). The mechanism is activated by the GPCR-agonist, PTH, which binds to PTH1R and activates $G\alpha_s$, which mediates the activation of cyclic AMP (cAMP) to turn on effector kinases (**Figure 9**). Activated PKA is responsible for the PTH-induced nuclear localization of αNAC where it affects bone-specific gene transcription (Pellicelli et al. 2014). In addition to activation by PTH signaling, the PKA-selective activator N^6-benzoyladenosine cAMP (6Bnz-cAMP) also leads to the translocation of αNAC from the cytosol to the nucleus (Pellicelli et al. 2014). The mechanism by which αNAC translocates to the nucleus where it regulates bone-specific gene transcription through a PTH-induced PKA-mediated action will be further detailed in the results. Both ILK and PKA induce the translocation of αNAC from the cytosol to the nucleus; however, it is not yet understood whether the phosphorylation of αNAC by ILK and PKA work in parallel or in series.

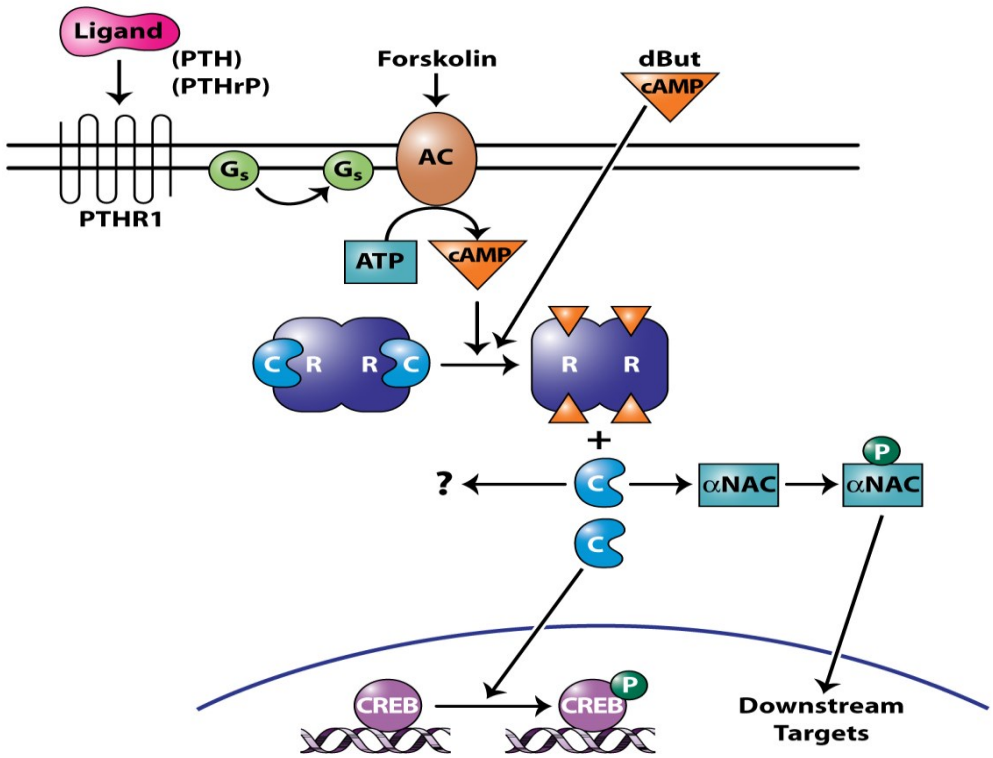

Figure 9. PTH activation of PKA leads to the nuclear localization of αNAC.

PTH acts as a GPCR agonist, binding to the PTH receptor (PTH1R). The binding of PTH to the receptor leads to the synthesis of cAMP via the binding of the $G\alpha_s$ subunit to adenylyl cyclase (AC). An increase in cytosolic cAMP activates PKA signaling (C), which in its inactive state is bound to its regulatory unit (R). Forskolin activates AC, which can also be used to activate c-AMP dependent pathways, such as PKA and the Epac pathways. Treatment with forskolin leads to an increase in cAMP levels, which in turn activates PKA. Dibutyryl-cAMP (dBut-cAMP) is a cAMP analogue, which is a non-specific activator of cAMP-sensitive pathways. Activated PKA phosphorylates αNAC at serine 99 (S99) in the cytosol leading to its nuclear localization and subsequent transcriptional activity as a coregulator where it can activate downstream targets. The cAMP response element-binding protein (CREB) is one such downstream target, where following PTH exposure CREB is phosphorylated and can stimulate the transcription of AP-1 activated genes (*c-Fos* and *c-Jun*). As previously discussed, αNAC can form a ternary complex with c-JUN and TBP to potentiate the transcription of *Ocn* gene expression (**Figure 6**).

1.3.4 Bone specific gene transcription induced by nuclear αNAC

The physiological role of αNAC in bone has been characterized using the S43A mutation knock-in mouse model (Meury et al. 2010). The introduction of a single point mutation, where serine residue 43 was mutated to an alanine, partially inhibits the nuclear translocation of αNAC. The S43A mutation exhibited decreased amounts of αNAC within the nucleus, remaining mainly in the cytosol. This in turn leads to less transcriptional activation by αNAC at the *Ocn* promoter. The S43A mutant mice exhibit decreased bone mass, more woven-type bone, and an increased number of osteocytes, and osteocyte markers resulting in an osteopenic phenotype (Meury et al. 2010). The S43A mutant knock-in mouse model shares a similar phenotype to the $G\alpha_s$ conditional knockout mouse model, in which $G\alpha_s$ has been deleted specifically from osteoblasts (Wu, Aarnisalo, and Bastepe 2011), as well as the $G\alpha_s$; αNAC compound heterozygote (Pellicelli et al. 2014). The $G\alpha_s$; αNAC compound heterozygote also exhibits reduced bone mass in trabecular bone, elevated expression of *Sost,* and increased cortical osteocyte number (Pellicelli et al. 2014). These data confirm the physiological role of αNAC in bone tissue and supports αNAC as a regulator of bone mass through a PTH-induced PKA-mediated mechanism.

II. Aims of study

- We plan to determine whether PTH triggers a PKA-dependent second messenger cascade to induce *Ocn* expression through an αNAC-regulated mechanism.
- Use high-throughput sequencing methods, in particular ChIP-seq and RNA-seq, to identify novel αNAC gene targets whose expression is influenced by PTH exposure.
- We concentrate on one αNAC gene target, *Lrp6,* and aim to show that PTH triggers a PKA-dependent second messenger cascade to induce *Lrp6* expression through an αNAC-regulated mechanism.

III. Materials and Methods

3.1 Reagents, antibodies, and cell lines

3.1.1. Reagents

PTH (1-34) (Catalog No. H4835) treatment was purchased from Bachem (Torrance, CA); Dibutyryl cAMP (Catalog No. D0627) N6-Benzoyladenosine cAMP (6Bnz; Catalog No. B009) were purchased from BioLog (Bremen, Germany).

3.1.2 Antibodies

Anti-αNAC (αNAC 1209), a polyclonal rabbit antibody raised against the recombinant αNAC protein recognizes the 35-kDa αNAC protein in nuclear extracts. This anti-αNAC antibody as previously described, recognizes both the phosphorylated and unphosphorylated form of αNAC (Yotov and St-arnaud 1996). αNAC 1209 was used in the ChIP-seq experiments.

Anti-Rabbit (Normal Rabbit IgG) was acquired from Santa Cruz (200µg/.5ml, Catalog No. SC-2027); 5.4µl per 1ml were added to each negative control in all ChIP assays.

Anti-αNAC-phosphoS99 antibody (pS99) is an affinity-purified rabbit polyclonal antibody raised against the peptide: NH2-TGVTRVTIRK-phosphoS-KNILFVITKP-COOH. It was produced by and purchased from PhosphoSolutions (Aurora, CO).

Anti-αNAC polyclonal chicken antibody raised against the recombinant αNAC protein was used in immunoblots of nuclear and cytoplasmic extracts (Meury et al. 2010).

A horseradish preoxidase conjugated anti-chicken secondary antibody (Southern Biotech) was used in all Western blots.

3.1.3 Cell line and subculturing

The preosteoblastic cell line, MC3T3-E1, was used for all cell culture experiments. MC3T3-E1 originates from mouse C57BL/6 calvaria (Sudo et al. 1983). The cells were cultured in α-Minimum essential media (αMEM, Catalog No. 12000-022, Life Technologies) containing 1mM L-Glutamine (Life Technologies, Burlington, ON) and 10% FBS (PAA Laboratories/GE Healthcare, Piscataway, NJ). MC3T3-E1 cells were grown to 85-95% confluency and passaged

at a ratio of 1:4 using Dubelco PBS (Catalog No.14190-144, Life technologies, Burlington, ON) and Gibco 0.05% Trypsin-EDTA 1X (Catalog No. 25300, Life technologies, Burlington, ON). For ChIP and DNA pull-down experiments cells were plated at approximately $1X10^6$ cells per plate.

shRNA knockdown in MC3T3-E1 cells

The shRNA protocol was developed by Hadla Hariri, and Dr. Martin Pellicelli. RNA samples were prepared by my colleague Hadla Hariri, PhD candidate. The shRNA generates a small hairpin, which effectively silences the expression of αNAC, by interfering with the RNA. Two shRNA hairpin constructs were created: shRNA1-αNAC 5'-CAAACGTATCAAGAGCAAAGG-3', and shRNA2-αNAC 5'-TACGAGAGTCACTATCCGAAA-3', and were cultured in HEK293 cells (Graham et al. 1977) with Dulbeco's modified Eagle's Medium (DMEM, Catalog No. 12800-017, Life technologies). Transfection was carried out via a calcium phosphate transfection protocol. αNAC knockdown was confirmed by both Western blot and PCR analysis, which confirmed the inhibition of αNAC expression. MC3T3-E1 cells incorporating the viral construct were selected by puromycin (5mg/ml). Following selection, MC3T3-E1 cells were treated with PTH, or water (Vehicle) for 2 hours.

3.2 Chromatin immunoprecipitation (ChIP)

Crosslinking

MC3T3-E1 cells were treated with either water (Vehicle), PTH (1-34), or 6Bnz. Cells were briefly fixated in the cell culture dish with the media for 10 minutes using 37% stock formaldehyde solution, with a final concentration of 1%. Glycine (0.125M final concentration) was added for five minutes to stop the crosslinking reaction. The cells were washed 2 times in cold 1X Phosphate-buffered saline (PBS). The cells were scraped and collected in cold PBS, and centrifuged in a Sorvall RT7 for 5 minutes at 2000 RPM.

Cell Lysis

The cells were resuspended in a series of lysis buffers to isolate the nuclei and remove

cytosolic proteins. The cells were passed through a 21 gauge needle in nucleus/chromatin preparation (NCP) buffer 1 (Hepes 10 mM pH 6.5, EDTA 10 mM, EGTA 0.5 mM, Triton X-100 0.25% v/v), and centrifuged in a Sorvall RT7 for 5 minutes at 2000 RPM at 4 ºC. The cells were then resuspended in NCP buffer 2 (Hepes 10 mM pH 6.5, EDTA 1 mM, EGTA 0.5 mM, NaCl 200 mM), and centrifuged in an Eppendorf 5415-R for 5 minutes at 2400 RPM at 4 ºC. The isolated nuclear pellet was resuspended in 200 µl of cold RIPA buffer A (150mM NaCl, 1% (v/v) NP-40, 0.5% (w/v) Na-deoxycholate, 0.5%(w/v) SDS, 50mM Tris-HCl pH 8.0, 5mM EDTA, 1mM PMSF, protease inhibitor (Catalog No. P8340, Sigma Aldrich)).

Sonication

The DNA strands were sheared by sonication for 18 cycles of 15-second pulses in an Ultrasonic dismembrator model 500 (Thermo Fisher Scientific, Waltham, MA) at 20% amplitude. ChIP samples to be sent for sequencing were sonicated for 30 cycles of 15-second pulses each at 20% amplitude. The difference in sonication time is due to the smaller fragment size required for sequencing (between 250-700bp). The lysate was centrifuged in an Eppendorf 5415-R at 13,000 RPM for 10 minutes to remove the debris. The supernatant was completed to 1ml with RIPA buffer B (150mM NaCl, 1% (v/v) NP-40, 0.5% (w/v) Na-deoxycholate, 0.1%(w/v) SDS, 50mM Tris-HCl pH 8.0, 5mM EDTA, 1mM PMSF, protease inhibitor).

Chromatin Immunoprecipitation

To prevent non-specific binding the nuclear lysate was pre-cleared for 1 hour with 30µl of protein G–streptavidin–agarose beads (Catalog No.17-0618-01, GE Healthcare Biosciences) per sample on a rotating wheel. The samples were then incubated with either an anti-αNAC antibody (1:50), anti-pS99 (1:10), or anti-rabbit (normal rabbit IgG) for 16 hours at 4 ºC on a rotating wheel. Fifty microliters of G–streptavidin–agarose beads were added to immunoprecipitate the target protein-DNA complex. The protein-DNA complex was rotated on the wheel at 4 ºC for 1 hour.

Wash and Elution

The protein-DNA complex was washed in a series of wash buffers: 2 times with cold RIPA buffer B, 4 times with cold lithium chloride buffer (100 mM Tris-HCl pH8.0, 500 mM LiCl, 1% (v/v) NP-40, 1% (w/v) deoxycholate), 2 times cold RIPA buffer B, and 1 time with TE (10 mM Tris-HCl pH 8.0, .1mM EDTA). The washed protein-DNA complex was then eluted by adding 150µl of 1% SDS to each sample. The samples were placed on a heating block at 65 ºC for ten minutes. The protein-DNA complex of interest was eluted from the beads, and the supernatant was transferred to new microcentrifuge tubes.

Decrosslinking

Crosslinking was reversed by heating the samples for 5 hours on a heating block at 65 ºC. Proteinase K (1.5µl of 10mg/ml), a serine protease which removes any contaminating proteins, was added to each sample during the 5 hour decrosslinking. The temperature was then lowered to 37 ºC for 30 minutes, and 1µl of Ribonuclease from bovine pancreas (Catalog No. R4642, Sigma-Aldrich) was added to each sample as an additional DNA purification step.

Extraction

The phenol-chloroform extraction works by removing unwanted protein and RNA in order to better isolate DNA. The sample volume was first increased to 400µl with TE. DNA extraction was carried out by adding 400µl of phenol:chloroform:isoamyl alcohol (Catalog No. 15593, Invitrogen) to each sample. Following vigorous shaking the samples were centrifuged for 15 minutes in an Eppendorf 5415-R at 13,000 RPM at 4 ºC. The aqueous layer was transferred to a new tube. 400µl of chloroform was added to each sample, and shaken vigorously prior to centrifugation. The samples were centrifuged for 15 minutes in an Eppendorf 5415-R at 13,000 RPM at 4 ºC. The aqueous layer was transferred to a new tube.

Precipitation

Glycogen from *Mytilus edulis* (1.5µl, Catalog No. G1767, Sigma-Aldrich) was added to each sample to assist with DNA precipitation. The ChIP product was precipitated overnight at -

20ºC in 1ml of 100% ethanol. The samples were centrifuged in an Eppendorf 5415-R for 15 minutes at 13000 RPM at 4 ºC. The samples were washed in 70% ethanol, air dried for 10-15 minutes, and resuspended in TE.

3.3 Sequencing analysis of ChIP products (ChIP-seq)

ChIP-sequencing (ChIP-seq) was performed by the McGill University and Genome Quebec Innovation Centre, Montreal, Canada. All samples were sequenced using the Illumina Hiseq 2000/2500 platform. There were three samples sequenced per condition, providing a triplicate set. The first step in the ChIP-seq pipeline is to trim all of the reads till they have received an appropriate Phred score, which calculates a logarithmic error probability that the base is correctly called. The Phred value assigns a score to the quality of the DNA sequence read. The trimming and clipping of reads was carried out using the Trimmomatic software. The reads are then aligned to the mouse reference genome. The alignment is carried out by the BWA software. This alignment generates binary alignment map (BAM) files, which are used as the input for filtering of the alignment quality by using the samtools program. The Homer software program is used to carry out the sequencing analysis by generating several quality metrics: (i) tag counts, (ii) tag autocorrelation (iii) sequence bias, and (iv) GC content bias. The peaks are called by using the MACS software. The peaks called are annotated using the RefSeq annotations. MACS also provides statistics on the peaks called, such as the number of peaks, the percentage near transcription start sites, and measurements on the peaks height and width. IGV software was used to further evaluate the nature of the peaks called, by loading the bedGraph track format files. IGV provided a visual comparison of the peaks called between different experimental conditions.

3.4 Analysis and quantification of ChIP product by RT-qPCR

Primer design

The ChIP products obtained from conventional ChIP assays were first validated for αNAC accumulation at the previously described murine *Ocn* promoter sequence by using RT-qPCR. Validation using the *Ocn* primers was considered a measure of positive control that the ChIP assay was functional. The *Ocn* primers used flank the αNAC DNA binding site: forward, 5'-TCGTCCACTCCCAGAGCCTTGC-3' reverse, 5-'CTGCACCCTCCAGCATCCAG-3 (Akhouayri, Quélo, and St-Arnaud 2005; Hekmatnejad et al. 2014). Following sequencing and the identification of novel αNAC DNA binding targets, primers were designed around the ChIP peak region using the sequences identified in IGV. Primers were made using the IDT DNA website using the primer quest software. Primer pairs were selected based on their proximity to the peak ChIP region, the primer pairs annealing temperature, hairpin TM, and percent GC content. Primers were designed around the murine *Lrp6* proximal promoter sequence, which flanks the peak region of the putative αNAC binding site (**Table 1**).

Gene	Forward 5'-3'	Reverse 5'-3'
Lrp6	GAAAGCGTAAGCCGCAATG	GTGGTCGGGACTACTTTCTG
Wdr34	CTCAAATGGCGCAAAGTACAG	GGAACAGCTCTTCGTGGTATAAG
Anp32e	AGGTGGGTGGAGTGTAGG	AGAGACGCAAAGACGAACG
Rbbp5	TCACGAAACTAAGTCAGACACATA	GCAGGAAAGCGGGAAAGG
Zfat	GACGTCGCAGCGTTCTG	CCACAGCCCTGGAAACTG
Epc1	GTCGCTGCCATTGTTGTG	TCGGAAAGAATGCACGACTG

Table 1. Forward and reverse primer sequences used to validate ChIP products by RT-qPCR.

The table includes six primer pairs that were designed and validated for the first six leading gene targets identified in the ChIP-seq.

The primers were validated by RT-qPCR using ChIP products to assess slope, R^2 value, Ct amplification, and dissociation curve. Assessment of these metrics ensure that the amplification of the ChIP product using the designed primers at the *Lrp6* promoter are efficient and of high quality. Additionally, primers were run on a 3% agarose gel with ethidium bromide to rule out the formation of primer dimers.

Validation by RT-qPCR

The ChIP product was amplified and detected using the SYBR green I master mix (Catalog No. 4309155, Applied Biosystems), which uses SYBR green dye, AmpliTaq Gold DNA polymerase, and dNTPs and dUTPs. The SYBR green master mix is combined with the ChIP input, ChIP experimental, and specific primers that amplify the DNA region of interest. The PCR instrument settings were as follows: one cycle of denaturation at 95 ºC for 10 minutes followed by 40 cycles at 95 ºC (15 s), 40 cycles at an annealing temperature of 60 ºC (60 s), and finally a terminal elongation and dissociation stage was carried out at 95 ºC (15 s), 60 ºC (60 s), and 95 ºC (15 s). The RT-qPCR SDS software (Applied Biosystems) generates a threshold cycle (Ct), which is the quantitative value at which the fluorescent probe exceeds the threshold. From the Ct value we can calculate the relative promoter occupancy of αNAC at the specific region of interest. This calculation indicates the amount of αNAC enrichment at the region of the promoter relative to the Vehicle ChIP (untreated) product. The ΔCt value normalizes the Ct values of the ChIP products to the reference input. ΔCt values were calculated by subtracting the Ct of the ChIP Input from the Ct of the corresponding ChIP experimental product; example ΔCt =Ct experimental - Ct Input. We then calculated the ΔΔCt value (ΔΔCt = ΔCt Experimental- Average ΔCt Vehicle Input). We evaluated the relative promoter occupancy in terms of fold change (Fold Change= $2^{-\Delta\Delta Ct}$). Quantification was carried out by running a triplicate of each ChIP input, and a duplicate of each ChIP experimental product. Relative quantification studies were pooled into triplicate sets for analysis.

3.5 DNA column Purification

The Quiagen DNA gel extraction kit (catalog No. 28706) was used to remove impurities from the ChIP samples prior to sequencing following the manufacturer's instructions. The purification kit works by adhering the DNA content onto a silica-membrane, and is subsequently washed then eluted from the spin-column membrane. A 10:1 ratio of of the binding QG buffer (5.5M guanidine thiocyanate, 20mM Tric-HCl pH 6.6) was added to each ChIP sample to bind it to the membrane.The sample was resuspended in a separate microcentrifuge tube, and then transferred to the spin column. The sample was spun for 1 minute at 13,000 RPM in an Eppendorf 5415-R. The flow through of the column was then discarded. Seven hundred fifty microliters of PE buffer (10mM Tris-HCl, pH 7.5, 80% ethanol) was added to each sample and left to stand on the bench for 2 minutes. The samples were then spun for 1 minute at 13,000 RPM in an Eppendorf 5415-R. The flow through was again discarded. The spin was repeated for 1 more minute to remove any of the residual wash buffer. The spin column was placed inside a new 1.5ml microcentrifuge tube. The DNA ChIP sample was eluted from the column by adding 50µl of elution buffer (10mM Tris-Cl pH 8.5, .5mM EDTA), and allowed to stand on the bench for 2 minutes prior to centrifugation. The purified samples were centrifuged for a final spin at 13000 RPM for 1 minute.

3.6 Quantification of samples for ChIP-seq by Picogreen Assay

The ChIP-seq samples were quantified using a Quant-iT PicoGreen dsDNA assay kit (Life Technologies, catalog No. P11496), which can quantify concentrations as low as 25pg/ml of dsDNA. A standard curve was established, beginning with a 2ng/µl concentration of the DNA standard. Eight serial dilutions were made, with a dilution factor of 1:4. The standard DNA solution was resuspended in TE Buffer. The 2µl of the ChIP samples were diluted in 48µl of TE (dilution of 1:25 for unknown samples). The PicoGreen reagent was prepared by first diluting the stock TE buffer (200mM Tris-HCl, 20 mM EDTA, pH 7.5) from 20X to 1X, and then

resuspending the 200X PicoGreen in TE for a final concentration of 1X. Each of the samples were resuspended in 50µl of the PicoGreen buffer for a total volume of 100µl. A flat black 96-well plate was used to load each sample. The plate was covered with aluminum foil and incubated for 2.5 minutes at room temperature. The plate was then read at 485nm excitation and 535nm emission.

3.7 Reverse Transcription

RNA extraction following PTH treatment in MC3T3-E1 cells

Adherent MC3T3-E1 cells were treated for either 1, 2, 6 or 8 hours with PTH (1-34). The cells were washed twice with 1X PBS under the hood. One milliliter of TRIzol reagent (Invitrogen, Catalog No. 15596-026) was added to each cell culture dish, and kept at room temperature for 2 minutes. The cells were then lifted from the dish and transferred to a 1.5ml microcentrifuge tube. The cells were stored at -80 °C prior to phase separation. Chloroform was added at a ratio of 0.2ml per 1ml of TRIzol to each sample. The samples were centrifuged 4°C at 12,000 RCF for 15 minutes in an Eppendorf 5415-R. The aqueous phase was transferred to a new set of sterile microcentrifuge tubes. The RNA was isolated by adding 0.5ml of 100% isopropanol to the aqueous phase. The samples were centrifuged at 12,000 RCF for 20 minutes at 4°C. The supernatant was removed and the RNA pellet was washed with 1ml of 75% ethanol. The isolated RNA pellet was centrifuged at 12,000 RCF for 5 minutes at 4°C. The wash was removed and the RNA pellet was air dried for 10 minutes. The isolated RNA was resuspended in 20µl of RNase-free water. RNA samples were quantified using the NanoDrop-1000 spectrophotometer (Thermo Fisher Scientific, Waltham, MA), with 1µg of RNA per sample to be reverse-transcribed. Reverse-transcription of RNA to cDNA was carried out using the High-Capacity cDNA reverse transcription kit (Applied Biosystems, Catalog No. 4368813) following the manufacturer's instructions. The 1µg RNA samples were made up to a volume of 20µl using a master mix containing random primers, multiscribe reverse transcriptase, and RNAse-free

water. The GeneAmp PCR 9700 thermal cycler (Applied Biosystems) was used to carry out the reverse-transcription from RNA to cDNA.

3.8 Relative quantification

Real-time quantitative PCR was carried out using the 7500 Real-time PCR system (Life Technologies Applied Biosystems) to monitor gene expression of cDNA samples. The 20µl cDNA samples were completed to a total volume of 100µl with TE buffer. Five percent of the cDNA was used along with 20µl of the TaqMan 2X Universal PCR master mix (Life Technologies, Catalog No.4326708), TaqMan Primers (B2M: Mm00607939-s1, RANK-L/Tnsf11: Mm00441908-m1, and Lrp6: Mm00999795-m1; acquired from Applied Biosystems), and sterile water. The thermal cycling regiment for the PCR were as follows: 2 min at 50°C, 10 min at 95°C, followed by 40 rounds of 15 s at 95°C and 1 min at 60°C. Beta-2 Microglobulin (B2M) was used as an endogenous reference gene.

The Ct values of the target gene of interest are normalized to its corresponding sample using the B2M as the endogenous control gene (ΔCt). In order to compare the normalized samples pertaining to the gene of interest we calculated the delta delta Ct (ΔΔCt) (Schmittgen and Livak 2008). The ΔCt value of the vehicle (untreated) samples was subtracted from the ΔCt of the treated samples (ΔΔCt= ΔCt treated-ΔCt vehicle). To evaluate gene expression, we calculated the normalized gene expression in terms of fold change (Fold Change= $2^{-\Delta\Delta Ct}$). Quantification of gene expression was carried out by running a duplicate of each sample, and each sample was part of a triplicate set for each condition.

3.9 RNA-Seq

RNA-sequencing was performed by the McGill University and Genome Quebec Innovation Centre, Montreal, Canada. All samples were sequenced using the Illumina Hiseq 2000/2500 platform. There were three samples sequenced per condition, providing a triplicate set. The

protocol used for preparing libraries was the firststrand TrueSeq mRNA protocol, which generated 108 to 134 million single reads per library. The Illimina CASAVA pipeline was used to determine the base calls. Base quality is encoded in Phred 33, which calculates a logarithmic error probability that the base is correctly called. This assigns a score to the quality of the DNA sequence read. The reads are then aligned to a reference genome. The percent of coverage is determined by the number of base pairs aligning to the reference genome divided by the total number of base pairs in the reference genome. The samples sequenced had a reported coverage of 77-94% coverage. Read counts were obtained using HTseq which reports the number of reads mapped to a given gene, and are later used as the inputs to determine the differential gene expression. The read counts are a measure of the linear abundance of the target transcript. The differential gene expression analysis is carried out using DESeq and edgeR R bioconductor package. We first examined the log fold change values of all of the αNAC ChIP-seq targets, and looked to see if these targets were statistically significant amongst the differentially expressed genes following PTH treatment. Additionally, we examined the p-value of these targets, and the adjusted p-value which takes into account the false discovery rate.

3.10 RNA column Purification

RNA column purification was carried out for samples to be submitted for sequencing. Total RNA extracted for RNA-seq was purified using the Qiagen RNeasy Mini Kit (Catalog No. 74104) following the manufacturer's instructions. The protocol uses silica-membrane based technology to adhere the RNA to the membrane via the RLT buffer (total composition of buffer is proprietary, contains a high concentration of guanidine isothiocycanate, which binds the RNA to the membrane). Purification is carried out by using the RPE buffer (total composition is proprietary, contains ethanol), which removes unwanted salts. The contaminants to the RNA can be washed away since the RNA is safely bound to the membrane. The RNA product is then

eluted in RNase-free water.

3.11 Nuclear extract and DNA pull-down assay

The objective of the nuclear extract and DNA pull down assay is to determine the protein-DNA binding location and sequence by capturing the complex with neutravidin biotinylated beads (Catalog No. 29200, Thermo Scientific). MC3T3-E1 plates were grown to 95% confluency. The cells were starved overnight in alpha-MEM media containing 1 mM L-glutamine and without FBS for 16 hours. Cells were treated for 1 hour with PTH. The cells were washed and collected in cold PBS. The cells were centrifuged in a Sorvall RT7 at 500g for 5 minutes at 4 ºC and resuspended in lysis buffer A (10mM HEPES pH 7.9, 1.5mM MgCl2, 10mM KCl, 1% NP-40, 500nM DTT, 1mM PMSF and protease inhibitor). During a 25-minute incubation on ice, the samples were vortexed every three minutes to disrupt the cytoplasm. They were then centrifuged at 600g in a Sorvall RT7 for 10 minutes at 4 ºC to isolate the crude nuclear fraction. The nuclear fraction was resuspended in 8ml of buffer B (50mM Tris Hcl pH 7.5, 2mM EDTA, 2MM EGTA, 1mM DTT, .1% Triton X-100, 1mM PMSF and protease inhibitor). This fraction was layered over 2ml of Buffer B containing 30% sucrose, and without Triton X-100. The samples were centrifuged at 3500g in a Sorvall RC-5B for 60 minutes at 4 °C. The pure nuclear fraction was resuspended in 350µl of buffer C (10mM Tris pH 7.5, 100mM KCl, 1mM EDTA, 500nM DTT, 5% Glycerol, .4% NP-40, 1mM PMSF and protease inhibitor). The pellet was then sonicated on ice for four 15-second pulses at 20% amplitude (Ultrasonic dismembrator model 500). The nuclear extract was centrifuged at 13,000g in an Eppendorf 5415-R for 10 minutes at 4 °C. The debris was discarded while the supernatant was transferred to a new tube for pre-clearing. The protein concentration was determined using a Bradford assay and the Beckman DU-640 spectrophotometer (GMI, Ramsey Minnesota). The absorbance of the standards and samples were measured at a wavelength of 595 nM. Two hundred fifty micrograms of protein underwent pre-clearing on a rotating wheel for 1.5 hours. The samples were spun down at 500g for 30 seconds, and the supernatant was transferred to a new tube. DNA probes flanking a

selected region of the ChIP peak proximal to the *Lrp6* promoter were prepared; 2µl of the forward and 2µl of the reverse biotinylated probes were completed with TE to 30 µl. The probes were boiled for five minutes and then cooled to room temperature. The supernatant containing 250µg of pre-cleared nuclear protein was transferred to the tubes containing the probes. 2µl of poly dI/dc was added to each sample as a non-specific competitor, and incubated on the shaker for 16 hours. The neutravidin agarose beads (Product # 29200 Thermo Scientific) were incubated overnight with 4µl of poly dI/dc in 1ml of buffer C. The nuclear protein complexes were recovered by incubating them for 1.5 hours at 4ºC with 50µl of neutravidin agarose beads. The protein-bead complex was washed 4 times in Buffer C and spun at 500g. The protein-bead complex was subsequently resolved by Western blot.

3.12 Western Blot

A Western blot assay was carried out to confirm the presence of the αNAC protein at a particular DNA binding site near the *Lrp6* promoter. The Western blot was carried out via a SDS-PAGE (Sodium Dodecyl Sulfate - PolyAcrylamide Gel electrophoresis), using a 12.5% polyacrylamide resolving gel to identify αNAC at 35-37 kDA.

Electrophoresis

A 12.5% acrylamide resolving gel (12.5% Acrylamide, .375M Tris pH 8.8, 0.1% SDS, 0.05% APS, TEMED) and 4% stacking gel (4% Acrylamide, .125M Tris pH 6.8, 0.1% SDS, 0.05% APS, TEMED) was prepared. The 250µg protein samples were prepared by adding 2x laemmli buffer and boiling them for five minutes. Running buffer (1X Tris-Glycine, .1% SDS) was added to the gel tank, and samples were run at 120V as they migrated through the stacking. The voltage was increased to 200V once the samples had entered the resolving gel.

Protein Transfer

The poly-acrylamide gel was transferred to a polyvinylidene fluoride membrane (PVDF, Millipore Ireland Ltd., County Cork, Ireland) using Whatman paper for backing (Whatman

International Ltd., Maidstone, England) and transfer buffer (70% water, 10% 10X Tris-Glycine, 20% Methanol) at 100V for 1.5 hours. The PVDF membrane was blotted in methanol and air-dried for 10 minutes. The membrane was then washed three times in Tris-Buffered Saline-Tween (TBST, 1X TBS, .1% Tween20) wash buffer. The membrane was blocked with 10% skim milk (TBST and skim milk powder) on a shaker at room temperature for 1 hour. The primary antibody, anti-αNAC (αNAC Chicken), was added to solution (1X PBST, 3% BSA, 0.02% Sodium Azide) at a concentration of 1:250 (40µl in 10ml), and incubated for 16 hours on a shaker at 4ºC. The primary antibody was removed and the PVDF membrane underwent 5 X 15 minute washes in TBST. A horseradish peroxidase conjugated anti-chicken secondary antibody (Southern Biotech) was added to a 5% skim milk solution at a concentration of 1:10,000, and the PVDF membrane was incubated with the secondary antibody on the shaker for 1 hour at room temperature. The membrane was subsequently washed 5 X 15 minute washes in TBST. The Western blots were developed using enhanced chemiluminescence (ECL, GE Healthcare Bio-Sciences, Baie d'Urfé, Quebec) following the manufacturer's instructions.

IV. Results

4.1 PTH exposure induces αNAC to accumulate at the *Ocn* promoter through a PKA-dependent second messenger pathway.

To examine whether PTH treatment, mediated by PKA, also induces the recruitment of endogenous αNAC at the *Ocn* promoter we performed quantitative ChIP assays on MC3T3-E1 cells. MC3T3-E1 cells were exposed to a 30-minute treatment with water (vehicle), 100nM PTH (1-34), or with the PKA-selective activator 6Bnz-cAMP (100μM). The ChIP assay used an anti-αNAC antibody (αNAC 1209), and the ChIP products were amplified via PCR using SYBR green. To identify promoter occupancy, primer pairs were used that flank the αNAC binding site of the *Ocn* proximal promoter (Hekmatnejad et al. 2014). Finally, the relative promoter occupancy was calculated as enrichment over vehicle-treated cells. The results indicate that the PTH-induced pathway stimulates the nuclear localization of αNAC, and a significant 5-fold enrichment of αNAC accumulation at the *Ocn* promoter. Treatment with the PKA-specific activator, 6Bnz-cAMP, induced a 6.5-fold enrichment of αNAC at the *Ocn* promoter (**Figure 10A**). A PKA-dependent mechanism is supported by additional assays carried out by Dr. Martin Pellicelli. Quantitaive ChIP assays were carried out in UMR-106 cells using a stably infected dominant negative form of PKA (PKAdn). PKAdn showed that PTH-induced enrichment of αNAC at the *Ocn* promoter is PKA-dependent, as inhibition of phosphorylation by PKA abolished significant accumulation of αNAC at the promoter (**Figure 10B**). Mutation of the phosphorylation site of αNAC (S99) by PKA to an unphosphorylatable site (S99A) demonstrated that PTH treatment induced phosphorylation at residue serine 99 for the PKA-mediated translocation of αNAC into the nucleus (**Figure 10C**). Finally, the transcriptional activation of *Ocn* is regulated by the phosphorylation of αNAC-S99. Luciferase assay studies using a phosphomimetic mutation (S99D) of αNAC enhanced the transcriptional activation of *Ocn* following PTH treatment as compared to the activity seen in the WT constructs. The S99A mutation demonstrated a loss of transcriptional activation of *Ocn* (**Figure 10D**). These results

demonstrate that PTH treatment induces the nuclear localization of αNAC, and the significant increase in relative promoter occupancy at the *Ocn* promoter upon the addition of 6Bnz-cAMP indicates that activation by the PTH pathway is PKA-dependent. Additionally, phosphorylation of αNAC by PKA occurs at residue serine 99, where this site is critical in the transcriptional activation of *Ocn* gene expression.

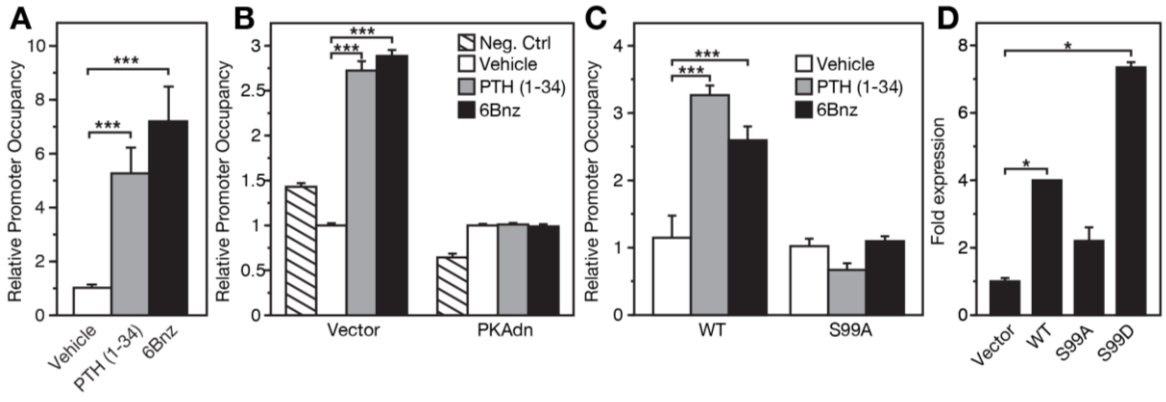

Figure 10. PTH induces the nuclear localization of αNAC at the Ocn promoter.
Endogenous αNAC translocates from the cytosol to the nucleus following 30-minute PTH (1-34) treatment in MC3T3-E1 cells. The accumulation of αNAC at the proximal promoter of *Ocn* demonstrated a significant 5-fold enrichment. The PKA-specific activator, 6Bnz-cAMP, exhibited a 6.5-fold enrichment. ChIP assays were carried out using αNAC 1209 and Normal Rabbit IgG antibodies. These results indicate that PTH treatment can induce the nuclear localization of αNAC, and subsequent occupancy by αNAC occurs at the *Ocn* promoter. Additionally, PKA mediates PTH-induced activation of the pathway as seen through the use of the PKA-specific activator, 6Bnz-cAMP (A). (B-C) Quantitative ChIP assays were carried out in UMR-106 cells. A dominant-negative form of PKA (PKAdn) expression vector was stably transfected into UMR-106 cells, with an empty expression vector used as the control. Controls expressing endogenous αNAC demonstrated significant enrichment of αNAC at the *Ocn* promoter, whereas enrichment by αNAC was abolished in cells expressing PKAdn (B). Phosphorylation of αNAC at S99 by PKA was further supported by carrying out ChIP assays on UMR-106 cells stably expressing FLAG-tagged WT and S99A αNAC. The S99A mutation inhibits phosphorylation of αNAC by PKA at this site (C). Enrichment of αNAC at the *Ocn* promoter is inhibited by the S99A mutation, supporting that phosphorylation by PKA at residue S99 is necessary for αNAC to localize to the nucleus and accumulate at the promoter of *Ocn.* Luciferase reporter gene assays were carried out on transiently-transfected UMR-106 cells. Cells were transfected with an *Ocn*-Luc reporter plasmid and three different expression vectors of WT or mutated αNAC: (i) c-JUN and WT, (ii) c-JUN and S99A, and (iii) c-JUN and S99D. Significant potentiation of *Ocn* gene expression by c-JUN and WT αNAC was found. The phosphomimetic S99D mutation

increased potentiation of *Ocn* gene expression. Loss of phosphorylation in S99A significantly reduced c-JUN mediated transcription of *Ocn* (D). The data shown in panel A is my own original work published in (Pellicelli et al. 2014).

4.2 Genome-wide analysis of αNAC binding sites indicates αNAC enrichment at the promoters of nine genes following PTH treatment.

Our first aim was to determine the genome-wide binding sites of αNAC using ChIP-seq to uncover DNA sequence motifs corresponding to αNAC network partners. *Ocn* is currently the best-characterized transcriptional target of αNAC. The ChIP-seq data provides us with a number of potential promoter targets that αNAC may interact with. The αNAC-specific rabbit polyclonal anti-αNAC antibody 1209 was used to immunoprecipitate the DNA fragments. Naïve IgG (Normal Rabbit IgG) was used as the negative control antibody. Sequencing analysis on the DNA fragments was performed at the McGill University and Génome Québec Innovation Centre, Montréal, Canada using the Illumina HiSeq 2000. Nine peak targets were identified as genes at which αNAC binds: *Lrp6, Wdr34, Anp32e, Zfat, Epc1, Rbbp5, Champ1, Tatdn3,* and *0610010K14RIK*. We focused on the first six genes as the peak expression of these genes was called multiple times when comparing PTH-treated versus negative control, and vehicle-treated versus negative control. The peak region of the gene targets ranged from 80-140 base pairs (bp). A typical result of peak regions identified by the ChIP-seq for one of the interesting gene targets*, Lrp6*, is shown in Figure 11. The sequencing peaks indicate putative DNA binding sites by αNAC near the promoter region of the respective genes. The peak region was annotated using IGV software, by inputting the start and end site of the bp number on each chromosome (Robinson et al. 2011). IGV software provides a visual map of where the gene resides on the chromosome (top track), as well as the location of genes identified by the RefSeq database annotations (bottom track). In many instances αNAC was detected as a peak in the untreated (Vhc) samples as well as the PTH-treated samples. As previously discussed, there are other mechanisms besides PTH that can lead to the translocation of αNAC into the nucleus. αNACs subsequent nuclear localization can lead to the activation of downstream targets. The antibody used (αNAC 1209) in the ChIP-seq experiments does not discriminate between various phosphorylated forms of αNAC; therefore, validation by ChIP using an antibody specific to the

PKA-mediated phosphorylated form of αNAC (αNAC-S99) is required to demonstrate that accumulation of αNAC at the promoter of *Lrp6* is due to a PKA-mediated mechanism. Our criteria for pursuing peak regions indicated by the ChIP-seq data is such that there is a significant difference between the peak region in the PTH-treated ChIP samples as compared to the negative control (**Figure 11**).

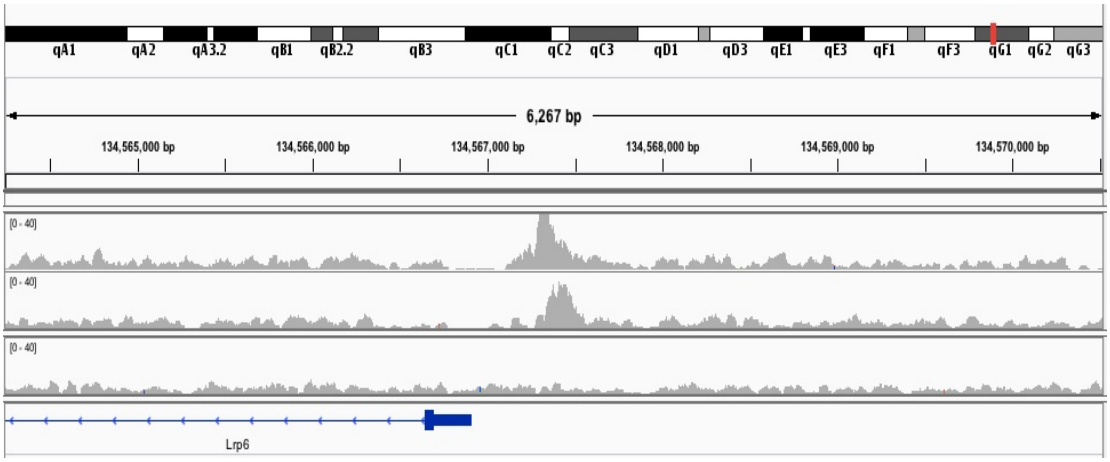

Figure 11. ChIP-seq peak identifies αNAC binding at the promoter of *Lrp6*.

Peak calling indicates an enrichment of aligned reads in a particular region of the genome. The height of the peak indicates that there is increased interaction in this region with αNAC and the genome. Presented here is a representative image using IGV from one of the triplicate studies. The top peak track is the PTH treated ChIP sample, the middle peak track is the vehicle treated sample, followed by the negative control at the bottom. The RefSeq genes are listed in the bottom track with the solid blue portion indicating the region of the *Lrp6* transcription start site. The red marking at qG1 indicates the location of *Lrp6* on the q arm of chromosome 6. We see enrichment of αNAC on chromosome 6:134567299-134567457 bp when compared to the background of the negative control. The RefSeq gene indicates this peak is located within the promoter region of *Lrp6*.

4.3 RNA-seq data confirms *Lrp6* is significantly modulated by PTH exposure.

Our first set of criteria in pursuing particular gene targets resulting from the ChIP-seq analysis was validation of the gene targets by RNA-seq. Both ChIP-seq and RNA-seq identify a wide range of targets; therefore, it is critical to validate that the gene target is first differentially expressed following PTH treatment. RNA-seq analysis was performed on MC3T3-E1 cells treated with PTH (1-34) for 1 hour. RNA was isolated following a TRIzol RNA extraction protocol, and purified in preparation for sequencing. Sequencing analysis was carried out by McGill University and Génome Québec Innovation Centre, Montréal, Canada using the illumina Hiseq 2000/2500 sequencer. Here we find that following PTH treatment *Lrp6* is differentially expressed with a p-value of 5.6×10^{-22}, and a log fold change of 1.103 (**Table 2**). *Lrp6* is a highly read target where the number of sequencing reads for the PTH samples double compared to the vehicle-treated cells. The statistical significance of *Lrp6* from the RNA-seq data further supports *Lrp6* as an appealing gene target of αNAC that is significantly modulated by PTH exposure in osteoblasts.

Gene Symbol	Log2 Fold Change	P-Value	PTH 1	PTH 2	PTH 3	Vhc 1	Vhc 2	Vhc 3
Lrp6	1.103	5.6e-22	22020	18343	21669	10081	9010	9788
Wdr34	-0.131	0.33	647	586	548	653	622	676
Anp32e	0.073	0.28	6282	5687	6174	6137	5532	5582
Zfat	-0.152	0.36	321	286	297	370	341	294
Epc1	-0.017	0.98	1405	1581	1633	1480	1600	1593
Rbbp5	-0.416	3.7e-05	1901	1798	1866	2518	2384	2524

Table 2. Validation of ChIP-seq targets with RNA-seq following 1-hour PTH treatment.
Six leading genes identified by ChIP-seq analysis were analyzed by using RNA-seq as potential gene targets that are modulated by PTH treatment. The RNA-seq was carried out by treating MC3T3-E1 cells with PTH (1-34) for 1 hour. The RNA-seq analysis indicated that both *Lrp6* and *Rbbp5* are significantly affected by PTH treatment, with a p-value of $5.6x10^{-22}$ and $3.7x10^{-5}$ respectively. The number of sequencing reads compared PTH-treated cells to the vehicle-treated cells. The number of sequencing reads for *Lrp6* approximately doubled for PTH samples compared to Vhc samples. Additionally, we observed a log fold change (Fold Change) of 1.103 for *Lrp6*; indicating that *Lrp6* expression is upregulated following PTH exposure.

4.4 PTH-induced binding of αNAC at the *Lrp6* promoter.

To validate that PTH induces accumulation of αNAC at the *Lrp6* promoter, we carried out conventional quantitative ChIP studies. The ChIP peak region was expanded 500 bp before and after the peak for the purpose of designing primers for validation by RT-qPCR. The primers used flank the *Lrp6* promoter and the putative αNAC binding site identified as a significant peak in our high-throughput ChIP-seq screen. We then used these primers in two quantitative ChIP studies of αNAC binding at *Lrp6*: one used an antibody directed against all forms of αNAC (αNAC 1209); another used an antibody directed against αNAC-S99, the form of αNAC that is phosphorylated in response to PTH-induced PKA signaling.

To design primers flanking the αNAC binding site at the *Lrp6* promoter, we incorporated the following criteria: (i) flank the ChIP peak region, (ii) encompass any putative αNAC binding sites, and (iii) identify enrichment of αNAC at the promoter of *Lrp6* following PTH treatment (**Figure 13**). The primers were evaluated for their efficiency first by PCR followed by an agarose gel to confirm the lack of primer-dimers. Detailed concentration assays were then performed to determine the optimal concentration combination for the forward and reverse primer pair.

The ChIP-seq analysis identified the potential region in which αNAC binds to the *Lrp6* promoter (**Figure 12**). The FASTA file sequence of each gene was analyzed in Snapgene viewer for putative αNAC binding sites. Based on the αNAC binding site sequence at the mouse *Ocn* promoter 5′-C/G C/G A C/G A C/G A nnn G-3 where n is any nucleotide, the degenerate sequence SSASASANNNG, or more loosely SSAVAVANNNG, was used to search for putative binding sites in the proximal promoter region of *Lrp6*. S represents either C or G; while V can be an A, C, or G but not T. Since the optimal αNAC binding sequence, GCACAGAGTAG, identified at the *Ocn* promoter was not found in the sequence of the *Lrp6* promoter, we focused on using a more relaxed form of the binding sequence to identify putative αNAC binding sites that could be experimentally verified.

In each quantitative ChIP study, MC3T3-E1 osteoblast cells were exposed to PTH (1-34), and the accumulation of αNAC at promoter of *Lrp6* was quantified using RT-qPCR. The response to PTH treatment was then compared to two control conditions: (i) an untreated control in which cells were exposed to the vehicle alone and not to PTH; and (ii) a negative control, in which cells were exposed to PTH, but an antibody directed against naïve IgG (rabbit) was used, rather than an αNAC-specific antibody.

Two separate sets of quantitative ChIP studies were carried out. In the first set of experiments, an antibody directed against all forms of αNAC was used (αNAC 1209), and cells were exposed to 100 nM PTH (1-34) for 30 minutes. In the second set of experiments, an antibody directed against the S99 form of αNAC (anti-pS99) was used, and cells were exposed to PTH for 1 hour. In both sets of experiments, the ChIP results for the PTH-treated cells were compared to both the untreated and negative controls described above.

PTH treatment for 30 minutes in which αNAC 1209 was used yielded a 1.5-fold enrichment of αNAC accumulation at the *Lrp6* promoter. Confirming that αNAC does indeed bind to the promoter of *Lrp6* (**Figure 13**). However, the amount of αNAC enrichment observed between the vehicle and PTH treated was not statistically significant at the 30-minute time point.

We then carried out ChIP assays using the anti-αNAC phospho-serine 99 antibody (pS99). The pS99 antibody used only binds to αNAC phosphorylated by PKA at serine 99. Two trials of ChIP assays revealed that following phosphorylation of αNAC at S99, which is a transcriptionally active form of αNAC shows significant accumulation at the *Lrp6* promoter. The relative occupancy of αNAC-S99 at the *Lrp6* promoter exhibits approximately a 5-fold enrichment compared to the positive and negative control (**Figure 14**). There are additional PTMs of αNAC that can lead to its nuclear localization and activation of downstream targets (Akhouayri, Quélo, and St-Arnaud 2005; Meury et al. 2010; Hekmatnejad et al. 2014). These concepts will be further detailed in the discussion. ChIP experiments using the rabbit polyclonal anti-αNAC antibody 1209 identifies all forms of endogenous αNAC. Therefore, to determine that

the accumulation of αNAC at the *Lrp6* promoter can be attributed to a PTH-induced PKA-mediated mechanism, subsequent ChIP experiments were carried out against the αNAC-S99 form.

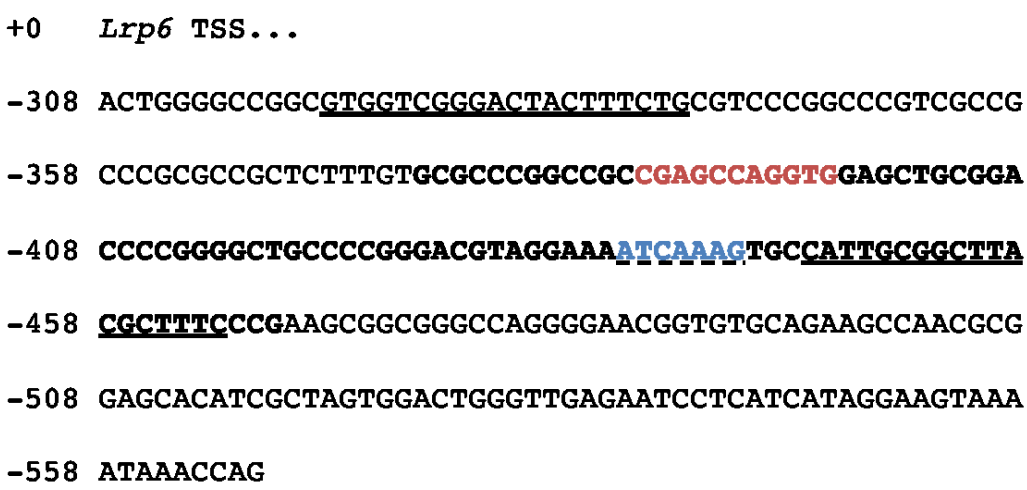

Figure 12. Sequence of the ChIP-seq peak region of the putative αNAC binding site in proximity to the *Lrp6* transcription start site.

ChIP-seq analysis revealed a peak region with a potential αNAC DNA binding site at the *Lrp6* promoter. The *Lrp6* transcription start site (TSS) is counted as 0 bp. A putative αNAC binding site is highlighted in red. The apex of the peak region is in bold and spans 93 bps. Forward and reverse primers were designed to flank the ChIP-seq peak region (solid underline) in order to amplify this region of the *Lrp6* promoter by PCR. The sequence highlighted in blue (dashed underline) is the predicted LEF1 consensus sequence, which is discussed in **Figure 15-16.**

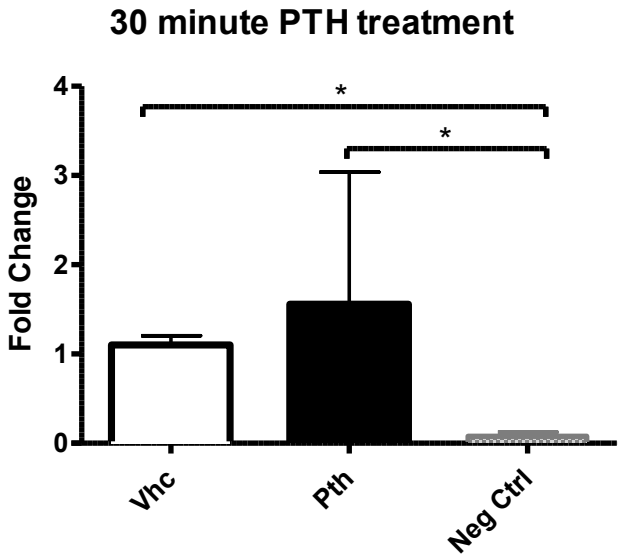

Figure 13. Endogenous αNAC binds to the promoter of *Lrp6* following PTH treatment. Conventional quantitative ChIP assays were performed following vehicle (Vhc) or 100nM PTH (1-34) treatment MC3T3-E1 cells. The cells were exposed to treatment for 30 minutes. Naïve IgG (rabbit) was used as a negative control. PTH treatment induced a 1.5-fold change of αNAC accumulation at the *Lrp6* promoter, as compared to the vehicle (Vhc) and negative control (Neg Ctrl). The data shown represent the mean ± SEM of a triplicate study. The groups were compared by one-way ANOVA, and a Bonferroni post-test. *, $P < 0.05$.

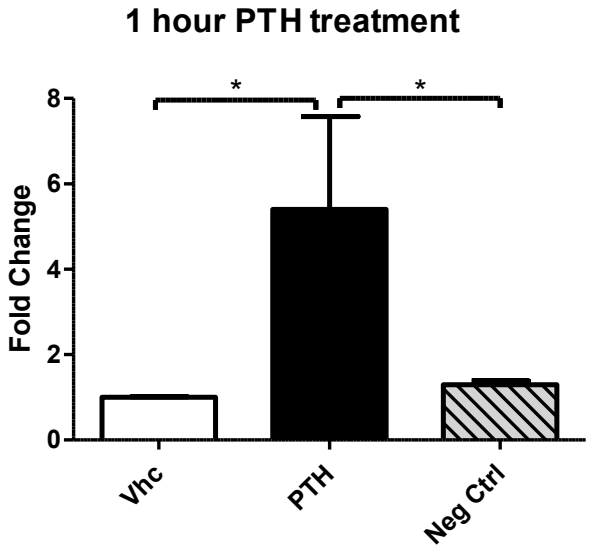

Figure 14. αNAC-S99 accumulates at the *Lrp6* promoter following PTH treatment. αNAC is phosphorylated at serine residue 99, where it localizes to the nucleus. The S99 phosphoacceptor site is activated by PTH treatment and mediated by PKA. Significant accumulation of the phosphorylated form of αNAC is seen at the promoter of *Lrp6* compared to the vehicle (Vhc) and negative control (Neg Ctrl). αNAC-S99 exhibits approximately a 5-fold change compared to controls. The data shown represent the mean ± SEM of two independent trials. The groups were compared by one-way ANOVA, and a Newman-Keuls post-test. *, $P < 0.05$.

4.5 **DNA pull-down assay indicates putative αNAC DNA binding site.**

Quantitative ChIP assays provide strong evidence that αNAC phosphorylated at S99 binds to the proximal promoter of *Lrp6.* A critical next step is to identify the precise DNA binding site of αNAC at the *Lrp6* promoter. This evidence will allow us to further our understanding of αNACs transcriptional regulation and activity of *Lrp6* gene expression. A DNA pull-down assay was carried out in order to isolate the nuclear material. We first generated probes that encompass the 93 bp ChIP peak region, as identified by the ChIP-seq analysis. The five probes spanned 190 bp, with the individual 50 bp probes overlapping one another by 15 bp (**Figure 15**). Each probe is labeled according to its bp distance away from the *Lrp6* promoter start site.

MC3T3-E1 cells were treated with 100nM PTH (1-34) for 1 hour to induce the translocation of αNAC from the cytosol to the nucleus. Cells were collected from the cell culture plates, and the nuclear extract was isolated following the DNA-pull down protocol. In addition to the five probes spanning the *Lrp6* ChIP peak region, 50 µg of nuclear extract and probes spanning the αNAC binding site at the *Ocn* proximal promoter were used as positive controls. A region with no known αNAC binding site near the *Ocn* gene was used as a negative control. The proteins were resolved by Western blot using an anti-αNAC (chicken) antibody. The αNAC protein has a molecular weight of 23 kDa, but runs at approximately 35-37 kDA when resolved by SDS-PAGE (Yotov and St-Arnaud 1996; Hekmatnejad et al. 2014). A representative blot from the DNA pull-down assay is used to demonstrate our initial findings (**Figure 16**). A signal is detected at 37 kDa within probe -413, as well as the OCN positive control, and a faint signal within the nuclear extract control (**Figure 16**). Moreover, no signal is detected in the OCN negative control. The signal within probe -413 is suggestive of a potential αNAC binding site. This finding was achieved twice; however further analysis by EMSA assay is needed to confirm the exact DNA-binding site of αNAC at the *Lrp6* promoter.

The 50 bp region of the -413 fragment probe was further investigated for other potential αNAC interaction partners at the promoter of *Lrp6*. A motif analysis of the 50 bp sequence was

carried out using the genomatix program MatInspector, which evaluates for transcription factor binding sites. The sequence of fragment probe -413 evaluated was the following: GGGCTGCCCCGGGACGTA**GGAAA<u>ATCAAAG</u>TGCCA**TTGCGGCTTACGCTT. The portion in bold revealed a TCF/LEF binding motif, and the underlined portion is the lymphoid enhancer-binding factor 1 (LEF1) consensus sequence (**Figure 11**). These preliminary results suggest that αNAC binds to the -413 fragment probe from the proximal *Lrp6* promoter following PTH treatment in osteoblast cells.

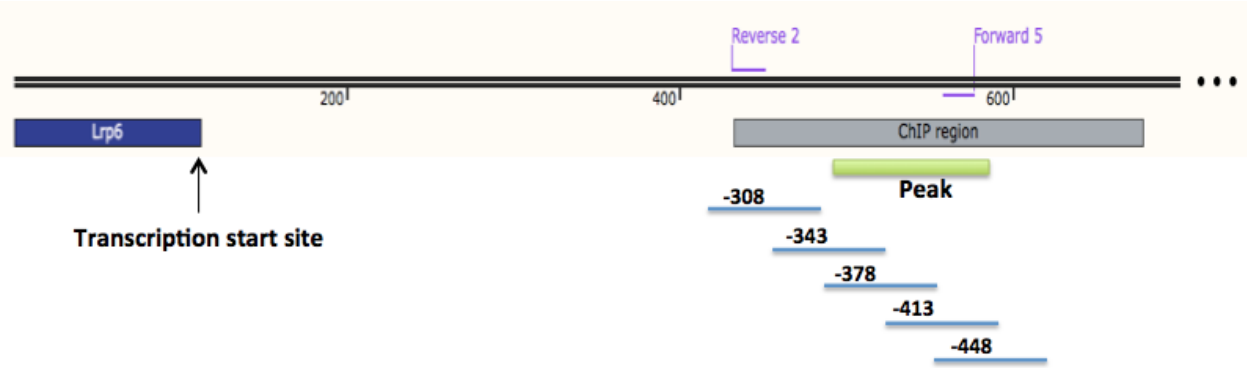

Figure 15. Map of the probes designed for the peak ChIP region for the DNA pull-down assays.

Five probes were designed around the 93 bp region (green), which is the apex of the peak region identified by the ChIP-seq analysis. The probes (light blue) are labeled in reference to their position to the *Lrp6* transcription start site (TSS) designated as 0 bp. The entire ChIP peak region is shaded in grey. Forward 5 and reverse 2 (purple) is the specific primer pair designed to amplify the ChIP product via PCR. Sequence motif analysis of probe -413 predicted a TCF/LEF binding motif with a LEF1 consensus sequence indicated (**Figure 12**, highlighted in blue).

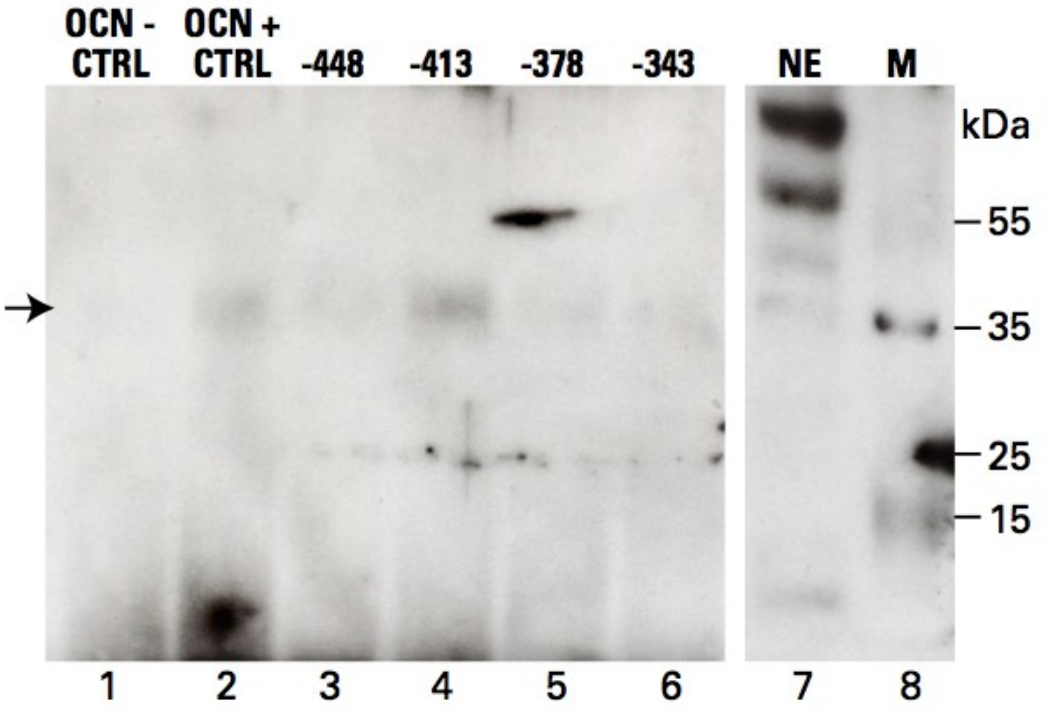

Figure 16. DNA pull-down assays reveal a putative αNAC binding site within probe -413. Proteins were resolved via Western blot following a DNA pull-down assay. The blot points to a putative αNAC binding site within probe -413; a signal was detected at approximately 37 kDa (arrow) using the anti-αNAC antibody. Furthermore, a positive signal was detected at the OCN positive control and in the 50 µg nuclear extract sample. The signal was absent in the OCN negative control.

Legend: NE, nuclear extract; M, marker of standard protein ladder; OCN + CTRL, OCN positive control; OCN - CTRL, OCN negative control.

4.6 A 2-hour treatment with PTH induces significant induction of *Lrp6* gene expression.

Time course experiments were carried out to assess the effect of PTH treatment and its ability to induce *Lrp6* gene expression over time. MC3T3-E1 cells underwent PTH (1-34) treatment for 2, 6 and 8 hours. At the end of the incubation the RNA was extracted via TRIzol extraction. Induction of *Lrp6* expression can be seen at 2 hours when compared to vehicle (water) treated cells, with a p-value less than 0.05. We find a similar inductive effect at the 2-hour time point in subsequent shRNA control experiments (see shRNA data, **Figure 18**). The 2-hour PTH treatment induced a 1.5 fold change compared to vehicle treated cells. However, the most significant inductive effect occurred at 6 hours with a p-value less than 0.001. Furthermore, the level of transcript enrichment remained stable over the 2, 6 and 8-hour time points (**Figure 17**).

The time course study was initiated to better understand the point at which the most significant induction occurred. RNA-seq data revealed that *Lrp6* induction occurred following only 1-hour PTH treatment (**Table 2**); indicating that *Lrp6* is an early gene target of PTH. Cell culture experiments validated by RT-qPCR as compared to the RNA-seq offer slight differences in the calculated fold changes, which can be attributed to the inherent differences in the assays used. Therefore, it is important to identify a specific time point at which future gene expression experiments should be carried out, validated by RT-qPCR.

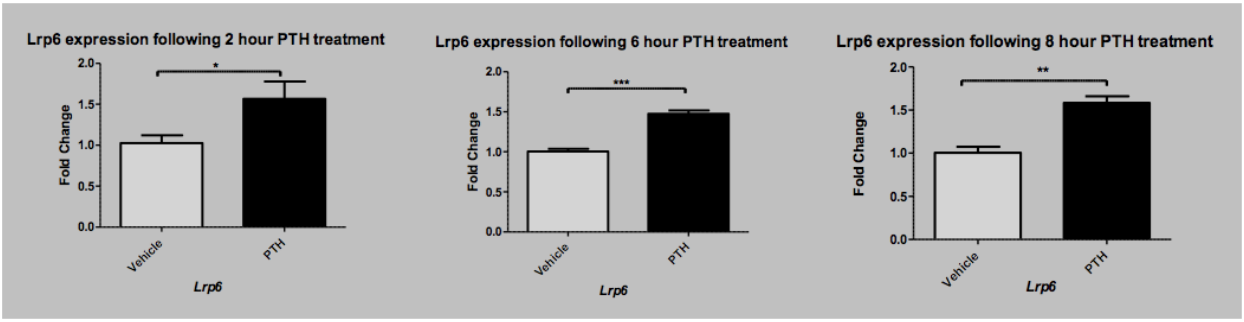

Figure 17. Time course study of *Lrp6* expression following PTH treatment.
MC3T3-E1 cells were treated with 100nM PTH (1-34) for 2, 6 or 8 hours. Following treatment RNA was extracted via TRIzol extraction protocol. Time course study evaluated the point at which significant *Lrp6* expression occurred. Induction is seen at 2-hours with a p-value of less than 0.05. Following 6-hour PTH treatment significant *Lrp6* expression is observed with a p-value of less than 0.001. 8-hour PTH treatment also induces significant *Lrp6* gene expression with a p-value less than 0.01. Statistical significance was assessed by t-test. *, $P < 0.05$; **, $P < 0.01$; ***, $P < 0.001$.

4.7 *Lrp6* gene expression is significantly reduced following shRNA knockdown of αNAC.

To test whether αNAC directly regulates *Lrp6* expression it was necessary to develop a tool in which endogenous αNAC expression could be inhibited. An shRNA platform to knockdown αNAC in MC3T3-E1 cells was developed in our lab by my colleague, Ms. Hadla Hariri, PhD candidate. Two specific shRNAs, namely shRNA 1 and shRNA 2, successfully inhibit αNAC mRNA and protein expression as demonstrated by RT-PCR and Western blot respectively (data not shown). Total RNA was extracted following the TRIzol extraction protocol, and gene expression was monitored by RT-PCR. Using this platform *Lrp6* transcripts were monitored in MC3T3-E1 cells following PTH treatment for 2 hours. PTH-treated cells transfected with the shRNA were compared to shRNA transfected MC3T3-E1 cells treated with water (vehicle) for 2 hours. The control set of samples used to evaluate the treatment arms in the shRNA were two different scrambled shRNA vectors on cells treated with either PTH or water.

Control samples treated with PTH for 2 hours exhibit a significant induction in *Lrp6* gene expression. Crucially, the loss of αNAC expression by shRNA consistently produced a significant reduction in the expression of *Lrp6* in PTH-treated cells, when compared to the PTH control (**Figure 18**). These results underscore the physiological relevance of αNAC as having significant transcriptional control over the induction of *Lrp6* gene expression in osteoblast cells following PTH treatment.

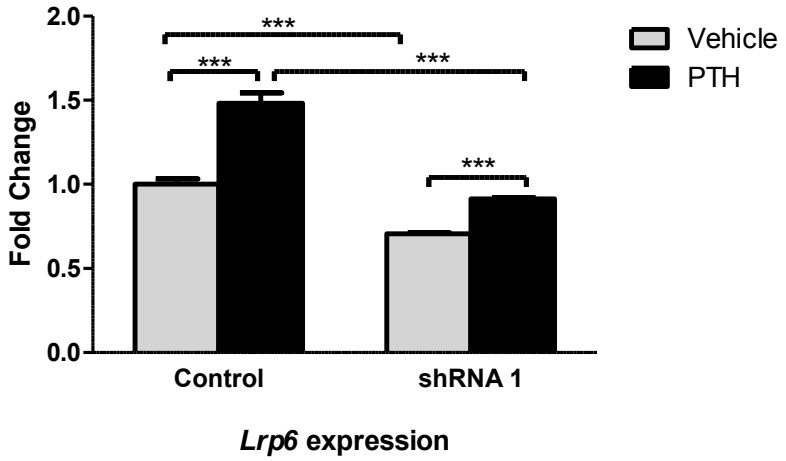

Figure 18. shRNA knockdown of endogenous αNAC significantly reduces the expression of *Lrp6.*

Endogenous αNAC expression is inhibited by shRNA 1 and shRNA 2. MC3T3-E1 cells were either vehicle or PTH-treated for 2 hours. Two-hour PTH treatment significantly induced enrichment of *Lrp6* transcripts. A significant reduction in *Lrp6* expression is demonstrated by the inhibition of αNAC through shRNA as compared to both vehicle and PTH controls. αNAC exerts significant transcriptional control over the induction of *Lrp6* gene expression.

A representative figure of a trial using shRNA1 carried out with triplicate measurements is presented here. shRNA 1 and shRNA 2 were used in triplicate experiments with triplicate measurements for each trial, and produced similar results. Statistical significance was assessed by two-way ANOVA, and a Bonferroni post-test. ***, $P < 0.001$.

V. Discussion

Previous research has shown that αNAC has an important role in bone development and is a key regulator of bone-specific gene transcription. In particular, αNAC functions as a transcriptional coactivator that regulates the expression of *Ocn.* Our study further elucidates the role of αNAC in regulating the expression of *Ocn* following exposure to PTH (Pellicelli et al. 2014). In addition, we have used high-throughput sequencing techniques that identified a number of novel potential gene targets of αNAC, among them *Lrp6*, an important component of the Wnt signaling pathway. Finally, we have sought to characterize the mechanism of transcriptional regulation that αNAC exerts on *Lrp6* expression. Our ongoing research on this problem is aimed at characterizing αNAC's interaction with the *Lrp6* promoter.

In our study, we have shown that PTH triggers a PKA-dependent second-messenger cascade to induce *Ocn* expression through an αNAC-regulated mechanism (Pellicelli et al. 2014). To examine whether PTH treatment, mediated by PKA, induces the recruitment of endogenous αNAC at the *Ocn* promoter we performed conventional quantitative ChIP assays on osteoblast cells. The significant accumulation of αNAC at the promoter of *Ocn* following PTH treatment supports the role of αNAC as an important coactivator of *Ocn* gene transcription (**Figure 10A**). The activation of *Ocn* gene expression is mediated through a PKA-dependent signaling cascade. The PKA-specific activator, 6Bnz-cAMP, supported the role of phosphorylation of αNAC by PKA to induce the activation of downstream targets. Inhibition of PKA using the dominant-negative form of PKA confirmed that PTH treatment induces the activation of PKA, which leads to the phosphorylation of αNAC at S99 (**Figure 10B**) (Pellicelli et al. 2014). αNAC-S99 is then capable of regulating *Ocn* gene expression, as well as other gene targets. *In vivo* studies further implicated αNAC as having an important role in affecting bone mass, where mouse models exhibited osteopenia, increased osteocyte number, and increased expression of *Sost* (Pellicelli et al. 2014). Finally, the design of this study provided the framework for approaching the characterization of αNAC-S99's regulation of novel gene targets.

Our high-throughput sequencing approach identified novel αNAC gene targets whose expression is influenced by PTH exposure. Previous research has suggested that there are additional gene targets regulated by αNAC (Meury et al. 2010; Jafarov, Alexander, and St-Arnaud 2012; Quélo, Prud'homme, and St-Arnaud 2004). Here we used genome-wide sequencing methods, in particular ChIP-seq and RNA-seq, to identify novel αNAC gene targets whose expression is modulated by PTH exposure. Through a bioinformatics analysis of our ChIP-seq data, we found 6 leading targets at which PTH significantly influenced αNAC's interactions with DNA across the mouse genome. To validate these ChIP-seq results, we carried out RNA-seq under similar conditions to determine that the targets identified were in fact influenced by PTH treatment. Of the targets identified by the high-throughput sequencing methods, *Lrp6* was an appealing gene target to pursue. LRP6 has already been shown to play a significant role in bone development via the Wnt signaling pathway, where *in vivo* mutant models exhibit disruption of osteoblast differentiation (Baron and Kneissel 2013). Following stimulation by PTH, the recruitment of LRP6 to the PTH/PTH1R/LRP6 ternary complex modulates the abundance of LRP6, which works to stabilize β-catenin in osteoblast cells. Finally, in LRP6-deficient mouse models the anabolic effects of PTH signaling on bone are greatly diminished (Wan et al. 2008; Li et al. 2013).

We show that PTH triggers a PKA-dependent second messenger cascade to induce *Lrp6* expression through an αNAC-regulated mechanism. To determine whether PTH exposure induces accumulation of αNAC at the promoter of *Lrp6*, we carried out conventional quantitative ChIP assays using both the anti-αNAC (αNAC 1209) antibody and anti-pS99 antibody. We found significant enrichment of αNAC-S99 accumulation at the promoter of *Lrp6* following 1-hour PTH treatment. These findings support that αNAC, when phosphorylated by PKA at residue serine 99, significantly accumulates at the promoter of *Lrp6.* We also detected binding of αNAC at the promoter of *Lrp6* with the pan-specific antibody αNAC 1209. However, the

difference between the accumulation of αNAC in PTH-treated cells and untreated cells did not reach statistical significance using that particular reagent.

There are number of post-translational modifications that αNAC undergoes that allows for its translocation to the nucleus. Different PTMs of αNAC can lead to the activation or repression of specific downstream targets (Meury et al. 2010; Hekmatnejad et al. 2014; Pellicelli et al. 2014). The endogenous αNAC antibody (αNAC 1209) identifies all forms of αNAC, and cannot discriminate between particular PTMs. It is therefore not surprising to see the translocation of αNAC into the nucleus in untreated samples, as there are alternate means for αNACs nuclear localization other than PTH treatment used in our study. Endogenous αNAC that enters the nucleus has the potential to activate downstream targets, which is one reason ChIP assays using αNAC 1209 antibody following 30-minute PTH treatment did not reach statistical significance (**Figure 13**). Therefore, antibodies raised against a particular PTM of αNAC are necessary to characterize the role the PTM has on αNACs regulation of bone-specific gene expression. ChIP assays using αNAC-pS99 antibody demonstrated that there was significant accumulation of αNAC at the *Lrp6* promoter following PTH treatment, as compared to endogenous αNAC in untreated samples, illustrating the importance of using antibodies against specific PTMs. We also find that a small proportion of unphosphorylated αNAC can enter the nucleus, as seen in the S43A mutant model (Meury et al. 2010), but its role in regulating gene expression is poorly understood at this time.

We show that there is a recruitment of αNAC at the promoter of *Lrp6*. To identify the precise DNA binding site of αNAC at the *Lrp6* promoter, we carried out a DNA pull-down assay. We identified a potential αNAC DNA-binding fragment (within probe -413) at the promoter of *Lrp6.* Interestingly, the 50 bp region identified as a potential binding site for αNAC did not contain a known or predicted αNAC response element. This led us to pursue the possibility of other potential interaction partners for αNAC. To identify other potential αNAC interaction partners within probe -413, we carried out a motif analysis using MatInspector. We identified eight

potential protein interaction partners that are predicted to bind the DNA sequence within the 50 bp region of the probe. One of the proteins identified with the highest sequence similarity was LEF1, which is currently our leading candidate as an interaction partner with αNAC, and is especially interesting given its role in regulating gene transcription in the Wnt signaling pathway.

shRNA studies in which αNAC expression is inhibited show that αNAC regulates *Lrp6* expression following PTH exposure. To assess the effect of PTH treatment and its ability to induce *Lrp6* gene expression over time, we first carried out a series of time-course experiments. We found that significant induction of *Lrp6* transcripts following PTH treatment occurred at 2 hours. To test whether αNAC directly regulates *Lrp6* expression we inhibited endogenous αNAC expression using shRNA. We found that 2-hour PTH treatment induced significant *Lrp6* gene expression in the control samples. Following PTH treatment, *Lrp6* expression is significantly reduced in osteoblasts in which αNAC expression is inhibited by shRNA. *Lrp6* expression is not completely inhibited in PTH-treated shRNA samples when compared to the vehicle-treated shRNA samples. This result is not unexpected, as it is well known that there are other mechanisms by which *Lrp6* expression can be activated following PTH exposure. However, a reduction in *Lrp6* expression following the knockdown of αNAC supports the hypothesis that αNAC directly regulates *Lrp6* expression following PTH treatment. An area requiring further investigation is the crosstalk between αNAC and other pathways, such as Wnt, and their activation of *Lrp6* gene expression.

Ongoing work

A critical next step in our study will be to identify whether αNAC directly binds the promoter of *Lrp6.* A classical approach to identifying protein-DNA binding interactions is the radioactive electrophoretic mobility shift assay (EMSA) (Hellman and Fried 2007). The radioactive assay is a more sensitive assay than the nonradioactive DNA pull-down approach we used in our study. One added advantage of the EMSA assay is that it can identify a single

nucleic acid sequence where multiple proteins, or a protein complex have bound. Since it is possible that αNAC may be co-localizing with other protein interaction partners at the *Lrp6* promoter region, EMSA would be a more efficient tool in identifying the nucleic acid sequence to which it binds.

Given that αNAC-S99 regulates the transcriptional activity of *Ocn* in a PTH-induced PKA-dependent manner, we suspected that αNAC-S99 also regulated the transcriptional activation of *Lrp6* (Pellicelli et al. 2014; Akhouayri, Quélo, and St-Arnaud 2005; Meury et al. 2010). To further characterize αNAC-S99's regulation of the transcriptional activity of *Lrp6* expression we plan to carry out luciferase assays using *Lrp6* promoter-driven luciferase reporters (Smale 2010). This luciferase gene, under the control of the *Lrp6* promoter, could be transfected into MC3T3-E1 cells with epitope-tagged expression vectors for WT or mutated forms of αNAC, such as the S99D and S99A mutations (Pellicelli et al. 2014). The luciferase assay studies will provide evidence for how αNAC influences the transcriptional activity of *Lrp6* expression in the presence of PTH.

In addition to the further characterization of αNAC's regulation of *Lrp6* expression, by EMSA and luciferase assays we are currently working towards optimizing a number of protocol conditions within our previous assays. In order to produce a more precise picture of how αNAC accumulates at the *Lrp6* promoter using quantitative ChIP assays, we have identified that it is necessary to extend the duration of PTH treatment. Initial ChIP assays examining the localization of endogenous αNAC at the promoter of *Lrp6* used only a 30-minute treatment time. This time point was used initially in order to replicate identical conditions used in the acquisition of the ChIP-seq data. However, we found from subsequent αNAC-S99 ChIP assays that 1-hour PTH treatment is a more suitable time point to induce statistically significant accumulation of αNAC at the promoter of *Lrp6.* Additional ChIP assays will examine the accumulation of endogenous αNAC at the *Lrp6* promoter following 1-hour PTH treatment.

In addition to the 6 leading gene targets identified by the preliminary bioinformatics

analysis of the ChIP-seq data, our lab has currently identified a number of additional putative αNAC gene targets that are affected by PTH-treatment. There is currently an ongoing effort within our lab to continue the validation and characterization of these additional αNAC gene targets that have been identified.

Future Studies

Our in vitro studies on αNAC's influence of *Ocn* and *Lrp6* expression in response to PTH support the hypothesis that αNAC plays an important role in mediating the activity of PTH and Wnt signaling in osteoblasts. Understanding the precise role of αNAC *in vivo* will require further studies in which organ-level or tissue-level phenotypes are characterized. To investigate the physiological relevance of αNAC binding at the *Lrp6* promoter, one promising strategy for further research is the development of murine mutants in which various aspects of αNAC signaling is disrupted. One model currently under development is the S99A knock-in mutant, where a serine to alanine mutation is knocked in at residue 99. This mutation would prevent αNAC from being phosphorylated at S99 by PKA, thus reducing its nuclear entry. Studies using the S99 mutant would allow us to determine the effect of αNAC's regulation of *Lrp6* on bone development. *In vivo* data that can be collected from the S99 knock-in murine model includes dynamic histomorphometry, immunohistochemistry, micro-computed tomography, and *in vivo* gene expression studies to evaluate gene expression of *Lrp6* at the tissue-level. We suspect that reduced nuclear entry of αNAC-S99 in the S99A model would lead to a reduction in *Lrp6* gene expression, and would subsequently have repercussions for regulating osteoblast gene expression, bone formation, and maintenance. Since there are still other mechanisms by which PTH treatment can induce an anabolic effect on bone formation, we would predict that the effect of PTH would be blunted in the S99A mouse model. Therefore, we would predict that the S99A model may lead to a low bone mass phenotype that would show an impaired response to the anabolic effect of PTH (Meury et al. 2010; Pellicelli et al. 2014; Li et al. 2013).

In our high-throughput sequencing studies we compared αNAC binding and gene expression in PTH treated and untreated osteoblasts. As in all high-throughput experiments, there are significant background levels of DNA binding and expression that needs to be corrected for when assessing the importance of αNAC-related signals. An additional set of RNA-seq experiments in which nuclear αNAC activity is greatly diminished, such as using the S99A knock-in mutation, or a knockdown of endogenous αNAC via shRNA, would be useful in identifying genes whose expression is reduced in the absence of nuclear αNAC. Additionally, N-ChIP assays, in which the chromatin remains "native" or uncrosslinked, would be useful in identifying whether the specific gene targets undergo certain histone modifications (O'Neill and Turner 2003). Evaluation of specific histone modifications can signal that the gene is transcriptionally active or silenced. For example, antibodies against sites of tri-methylation of Histone H3 at lysine 4 are used to immunoprecipitate a transcriptionally active region of euchromatin, while antibodies against tri-methylation of Histone H3 at lysine 9 are transcriptionally silenced regions (Kouzarides 2007). These additional high-throughput studies would therefore be informative, and would potentially allow us to identify with greater confidence a larger number of αNAC's gene targets that are modulated by PTH exposure and their transcriptional activity due to αNAC's binding.

Previous work has shown that αNAC can directly bind DNA, and that its DNA-binding domain (DBD) is required for the potentiation of AP-1 mediated *Ocn* gene expression (Akhouayri, Quélo, and St-Arnaud 2005). However, it is known that there are also cases in which the binding of the αNAC DBD is not required for the regulation of gene transcription (Meury et al. 2010). For example αNAC functions as a transcriptional coactivator by binding to c-JUN, which mediates the transcription of the α_1(I) collagen gene (*Collα1*). Deletion of the αNAC DBD indicated that the DBD was not necessary for coactivation by αNAC at the *Collα1* promoter. These experiments indicate that αNAC can be recruited through protein-protein

interactions without binding of the DBD where it can act as a coactivator for bone-related gene transcription (Meury et al. 2010).

Conventional ChIP alone cannot distinguish between αNAC that is bound to DNA directly, or through a DNA-bound interaction partner. This limitation arises because the formaldehyde fixative agent used in ChIP assays will also capture proteins that are strongly bound to proteins in close proximity to the region of chromatin being isolated. For this reason, additional techniques are required to determine whether gene transcription is regulated by αNAC as a DNA-bound coregulator, or through the formation of a protein-DNA complex. One way to reconcile this limitation is through the use of the ChIP-reChIP assay, which is an example of a technique that can determine the presence of protein complexes in the presence of a particular genomic region (Furlan-Magaril, Rincón-Arano, and Recillas-Targa 2009). This technique works by carrying out the first immunoprecipitation using one of the complexes antibodies, and then subjecting the isolated chromatin to a second round of immunoprecipitation with a second antibody ultimately leaving only chromatin where both proteins have bound. Using the ChIP-reChIP assay, we can determine whether αNAC binds the promoter region of *Lrp6* directly, or whether αNAC regulates *Lrp6* expression by complexing with another DNA-bound protein.

While ChIP-reChIP identifies members of such complexes it cannot distinguish the DNA-binding sequences, as assays such as EMSA can. As previously discussed, EMSA can specifically identify the binding sequences of such complexes, and aid in delineating the role of certain portions of DNA binding sequences by mutating portions of the sequence. Finally, luciferase assays using expression vectors in which the αNAC DBD is mutated can help determine whether the binding domain is transcriptionally active and necessary for the potentiation of gene expression, or whether αNAC binding to a protein-DNA complex is sufficient for the regulation of gene expression.

Our study also raises questions about how other endocrine signals might influence osteoblast activity in concert with PTH. It has been established that PTH influences many other signaling pathways in osteoblasts, among them the Wnt signaling pathway of which LRP6 is an important component (Li et al. 2013; Wan et al. 2008; Baron and Kneissel 2013). Other important pathways influenced by PTH include TGFβ and BMP signaling (Li et al. 2013). One especially interesting issue is whether αNAC has a role in integrating signals from disparate pathways related to energy metabolism, as suggested by OCN's connections to leptin and insulin signaling (Lee et al. 2007; Ducy et al. 2000; Hinoi et al. 2008).

Additional *in vivo* and *in vitro* work will be necessary to fully elucidate the mechanism by which αNAC regulates *Lrp6* expression. Previous studies demonstrated that LRP6 is critical in mediating PTH-induced activation of $G\alpha_s$-PKA signaling cascade (Wan et al. 2011). One potential mechanism is the existence of a positive feedback loop between LRP6-mediated activation of the PKA signaling cascade resulting in the activation of *Lrp6* by αNAC following its phosphorylation by PKA. LRP6 is critical in transducing the anabolic effect of PTH signaling, which suggests that insufficient activation by LRP6 complexing with PTH would result in modulation of αNAC activity. Furthermore, investigating the role of αNAC in osteoblast-specific LRP6-deficient mice may yield another level of understanding in αNAC's regulation of *Lrp6* expression (Li et al. 2013). In LRP6-deficient mice, we may expect to find diminished activation $G\alpha_s$-PKA signaling cascade, resulting in reduced nuclear entry of αNAC-S99.

The binding of αNAC to the promoter of *Lrp6* provides evidence that αNAC plays a role in regulating key factors in the Wnt signaling pathway. This raises the question whether αNAC's activity in the nucleus provides feedback signals to the Wnt signaling pathway. Additional studies will be required to uncover whether αNAC following PTH exposure works in concert with Wnt to activate *Lrp6* expression, and whether activation by a specific agonist (PTH vs Wnt) results in a different physiological outcome. Additional research will also be needed to determine whether αNAC influences other Wnt signaling components besides *Lrp6*. LRP6 can

complex with the PTH-PTH1R without input from Wnt signals (Baron and Kneissel 2013), therefore it is also possible that αNAC functions as a backup parallel pathway to ensure there is sufficient production of a critical protein required for proper bone formation and maintenance. Our hope is that further understanding of the crosstalk between the PTH and Wnt signaling pathways may yield new insights into the role of osteoblasts in bone development and homeostasis. A deeper understanding of the role of αNAC in mediating this and other interactions between PTH and other key signaling pathways may lead ultimately to novel druggable targets for the treatment of osteoporosis and other bone diseases.

References

Akhouayri, Omar, Isabelle Quélo, and René St-Arnaud. 2005. “Sequence-Specific DNA Binding by the A NAC Coactivator Is Required for Potentiation of c-Jun-Dependent Transcription of the Osteocalcin Gene.” *Molecular and Cellular Biology* 25 (9): 3452–60. doi:10.1128/MCB.25.9.3452.

Andersen, Thomas Levin, Teis Esben Sondergaard, Katarzyna Ewa Skorzynska, Frederik Dagnaes-Hansen, Trine Lindhardt Plesner, Ellen Margrethe Hauge, Torben Plesner, and Jean-Marie Delaisse. 2009. “A Physical Mechanism for Coupling Bone Resorption and Formation in Adult Human Bone.” *The American Journal of Pathology* 174 (1): 239–47. doi:10.2353/ajpath.2009.080627.

Baek, WY, and JE Kim. 2010. “Transcriptional Regulation of Bone Formation.” *Frontiers in Bioscience (Scholar Edition)* S3: 126–35. http://scholar.google.com/scholar?hl=en&btnG=Search&q=intitle:No+Title#0.

Baron, Roland, and Michaela Kneissel. 2013. “WNT Signaling in Bone Homeostasis and Disease: From Human Mutations to Treatments.” *Nature Medicine* 19 (2). Nature Publishing Group: 179–92. doi:10.1038/nm.3074.

Baron, Roland, and Georges Rawadi. 2007. “Wnt Signaling and the Regulation of Bone Mass.” *Current Osteoporosis Reports* 5 (2): 73–80. http://www.ncbi.nlm.nih.gov/pubmed/17521509.

Bellido, T., A.A. Ali, I. Gubrij, L. I. Plotkin, Q. Fu, C. a. O’Brien, S. C. Manolagas, and R. L. Jilka. 2005. “Chronic Elevation of Parathyroid Hormone in Mice Reduces Expression of Sclerostin by Osteocytes: A Novel Mechanism for Hormonal Control of Osteoblastogenesis.” *Endocrinology* 146 (11): 4577–83. doi:10.1210/en.2005-0239.

Bellido, Teresita, A Afshan Ali, Lilian I Plotkin, Qiang Fu, Igor Gubrij, Paula K Roberson, Robert S Weinstein, Charles a O’Brien, Stavros C Manolagas, and Robert L Jilka. 2003. “Proteasomal Degradation of Runx2 Shortens Parathyroid Hormone-Induced Anti-Apoptotic Signaling in Osteoblasts. A Putative Explanation for Why Intermittent Administration Is Needed for Bone Anabolism.” *The Journal of Biological Chemistry* 278 (50): 50259–72. doi:10.1074/jbc.M307444200.

Boyce, Brendan F, and Lianping Xing. 2008. “Functions of RANKL/RANK/OPG in Bone Modeling and Remodeling.” *Archives of Biochemistry and Biophysics* 473 (2): 139–46. doi:10.1016/j.abb.2008.03.018.

Clarke, Bart. 2008. “Normal Bone Anatomy and Physiology.” *Clinical Journal of the American Society of Nephrology : CJASN* 3 Suppl 3 (November): S131–39. doi:10.2215/CJN.04151206.

DiGirolamo, Douglas J, Thomas L Clemens, and Stavroula Kousteni. 2012. “The Skeleton as an Endocrine Organ.” *Nature Reviews. Rheumatology* 8 (11). Nature Publishing Group: 674–83. doi:10.1038/nrrheum.2012.157.

Ducy, Patricia, Michael Amling, Shu Takeda, and Matthias Priemel. 2000. “Leptin Inhibits Bone Formation through a Hypothalamic Relay: A Central Control of Bone Mass.” *Cell* 100: 197–207.

Ducy, Patricia, and Gérard Karsenty. 1995. “Two Distinct Osteoblast-Specific Cis -Acting Elements Control Expression of a Mouse Osteocalcin Gene.” *Molecular and Cellular Biology* 15 (4): 1858–69.

Ducy, Patricia, Rui Zhang, V Geoffroy, AL Ridall, and G Karsenty. 1997. “Osf2/Cbfa1: A Transcriptional Activator of Osteoblast Differentiation.” *Cell* 89: 747–54.

Franz-Odendaal, TA. 2011. “Induction and Patterning of Intramembranous Bone.” *Frontiers in Bioscience (Landmark Edition)* 16 (1): 2734–46.

Furlan-Magaril, Mayra, Héctor Rincón-Arano, and Félix Recillas-Targa. 2009. “DNA-Protein Interactions.” *Methods in Molecular Biology, DNA-Protein Interactions* 543: 253–66. doi:10.1007/978-1-60327-015-1.

Graham, F. L., J. Smiley, W. C. Russell, and R. Nairn. 1977. "Characteristics of a Human Cell Line Transformed by DNA from Human Adenovirus Type 5." Journal of General Virology 36: 59-72.

Håkelien, AM, JC Bryne, and KG Harstad. 2014. “The Regulatory Landscape of Osteogenic Differentiation.” *Stem Cells* 32: 2780–93. doi:10.1002/stem.1759.

Hartmann, Christine. 2006. “A Wnt Canon Orchestrating Osteoblastogenesis.” *Trends in Cell Biology* 16 (3): 151–58. doi:10.1016/j.tcb.2006.01.001.

Hekmatnejad, Bahareh, Omar Akhouayri, Toghrul Jafarov, and René St-Arnaud. 2014. “SUMOylated αNAC Potentiates Transcriptional Repression by FIAT.” *Journal of Cellular Biochemistry* 115 (5): 866–73. doi:10.1002/jcb.24729.

Hellman, Lance M, and Michael G Fried. 2007. “Electrophoretic Mobility Shift Assay (EMSA) for Detecting Protein-Nucleic Acid Interactions.” *Nature Protocols* 2 (8): 1849–61. doi:10.1038/nprot.2007.249.

Hinoi, Eiichi, Nan Gao, Dae Young Jung, Vijay Yadav, Tatsuya Yoshizawa, Martin G Myers, Streamson C Chua, Jason K Kim, Klaus H Kaestner, and Gerard Karsenty. 2008. “The Sympathetic Tone Mediates Leptin’s Inhibition of Insulin Secretion by Modulating Osteocalcin Bioactivity.” *The Journal of Cell Biology* 183 (7): 1235–42. doi:10.1083/jcb.200809113.

Hodsman, Anthony B, Douglas C Bauer, David W Dempster, Larry Dian, David a Hanley, Steven T Harris, David L Kendler, et al. 2005. “Parathyroid Hormone and Teriparatide for the Treatment of Osteoporosis: A Review of the Evidence and Suggested Guidelines for Its Use.” *Endocrine Reviews* 26 (5): 688–703. doi:10.1210/er.2004-0006.

Iwaniec, Urszula T, Thomas J Wronski, Jeff Liu, Mercedes F Rivera, Rosemarie R Arzaga, Gwenn Hansen, and Robert Brommage. 2007. “PTH Stimulates Bone Formation in Mice

Deficient in Lrp5." *Journal of Bone and Mineral Research* 22 (3): 394–402. doi:10.1359/jbmr.061118.

Jafarov, Toghrul, James W M Alexander, and René St-Arnaud. 2012. "αNAC Interacts with Histone Deacetylase Corepressors to Control Myogenin and Osteocalcin Gene Expression." *Biochimica et Biophysica Acta* 1819 (11): 1208–16. doi:10.1016/j.bbagrm.2012.10.005.

Jensen, ED, R Gopalakrishnan, and JJ Westendorf. 2010. "Regulation of Gene Expression in Osteoblasts." *Biofactors* 36 (1): 25–32. doi:10.1002/biof.72.Regulation.

Jilka, Robert L. 2007. "Molecular and Cellular Mechanisms of the Anabolic Effect of Intermittent PTH." *Bone* 40 (6): 1434–46. doi:10.1016/j.bone.2007.03.017.

Karsenty, Gérard, and Mathieu Ferron. 2012. "The Contribution of Bone to Whole-Organism Physiology." *Nature* 481 (7381): 314–20. doi:10.1038/nature10763.

Karsenty, Gérard, Henry M Kronenberg, and Carmine Settembre. 2009. "Genetic Control of Bone Formation." *Annual Review of Cell and Developmental Biology* 25: 629–48. doi:10.1146/annurev.cellbio.042308.113308.

Karsenty, Gerard, and Erwin F Wagner. 2002. "Reaching a Genetic and Molecular Understanding of Skeletal Development." *Developmental Cell* 2 (4): 389–406. http://www.ncbi.nlm.nih.gov/pubmed/11970890.

Knothe Tate, Melissa L, Josée R Adamson, Andrea E Tami, and Thomas W Bauer. 2004. "The Osteocyte." *The International Journal of Biochemistry & Cell Biology* 36 (1): 1–8. doi:10.1016/S1357-2725(03)00241-3.

Kollet, Orit, Ayelet Dar, Shoham Shivtiel, Alexander Kalinkovich, Kfir Lapid, Yejezkel Sztainberg, Melania Tesio, et al. 2006. "Osteoclasts Degrade Endosteal Components and Promote Mobilization of Hematopoietic Progenitor Cells." *Nature Medicine* 12 (6): 657–64. doi:10.1038/nm1417.

Komori, T, H Yagi, S Nomura, and A Yamaguchi. 1997. "Targeted Disruption of Cbfa1 Results in a Complete Lack of Bone Formation Owing to Maturational Arrest of Osteoblasts." *Cell* 89 (5): 755–64. doi:10.1016/S0092-8674(00)80258-5.

Kouzarides, Tony. 2007. "Chromatin Modifications and Their Function." *Cell* 128 (4): 693–705. doi:10.1016/j.cell.2007.02.005.

Kramer, Günter, Daniel Boehringer, Nenad Ban, and Bernd Bukau. 2009. "The Ribosome as a Platform for Co-Translational Processing, Folding and Targeting of Newly Synthesized Proteins." *Nature Structural & Molecular Biology* 16 (6): 589–97. doi:10.1038/nsmb.1614.

Lee, Na Kyung, Hideaki Sowa, Eiichi Hinoi, Mathieu Ferron, Jong Deok Ahn, Cyrille Confavreux, Romain Dacquin, et al. 2007. "Endocrine Regulation of Energy Metabolism by the Skeleton." *Cell* 130 (3): 456–69. doi:10.1016/j.cell.2007.05.047.

Li, Changjun, Qiujuan Xing, Bing Yu, Hui Xie, Weishan Wang, Chenhui Shi, Janet L Crane, Xu Cao, and Mei Wan. 2013. “Disruption of LRP6 in Osteoblasts Blunts the Bone Anabolic Activity of PTH.” *Journal of Bone and Mineral Research* 28 (10): 2094–2108. doi:10.1002/jbmr.1962.

Marie, Pierre J. 2008. “Transcription Factors Controlling Osteoblastogenesis.” *Archives of Biochemistry and Biophysics* 473 (2): 98–105. doi:10.1016/j.abb.2008.02.030.

Meury, Thomas, Omar Akhouayri, Toghrul Jafarov, Vice Mandic, and René St-Arnaud. 2010. “Nuclear Alpha NAC Influences Bone Matrix Mineralization and Osteoblast Maturation in Vivo.” *Molecular and Cellular Biology* 30 (1): 43–53. doi:10.1128/MCB.00378-09.

Moreau, Alain, Wagner V Yotov, Francis H Glorieux, and René St-Arnaud. 1998. “Bone-Specific Expression of the Alpha Chain of the Nascent Polypeptide-Associated Complex, a Coactivator Potentiating c-Jun-Mediated Transcription.” *Molecular and Cellular Biology* 18 (3). American Society for Microbiology: 1312–21.

Morvan, Frederic, Kim Boulukos, Philippe Clément-Lacroix, Sergio Roman Roman, Isabelle Suc-Royer, Béatrice Vayssière, Patrick Ammann, et al. 2006. “Deletion of a Single Allele of the Dkk1 Gene Leads to an Increase in Bone Formation and Bone Mass.” *Journal of Bone and Mineral Research* 21 (6): 934–45. doi:10.1359/jbmr.060311.

Mundlos, S, F Otto, C Mundlos, J.B Mulliken, a.S Aylsworth, S Albright, D Lindhout, et al. 1997. “Mutations Involving the Transcription Factor CBFA1 Cause Cleidocranial Dysplasia.” *Cell* 89 (5): 773–79. doi:10.1016/S0092-8674(00)80260-3.

Nakashima, Kazuhisa, Xin Zhou, Gary Kunkel, and Zhaoping Zhang. 2002. “The Novel Zinc Finger-Containing Transcription Factor Osterix Is Required for Osteoblast Differentiation and Bone Formation.” *Cell* 108 (1): 17–29. doi:10.1016/S0092-8674(01)00622-5.

O’Neill, Laura P., and Bryan M. Turner. 2003. “Immunoprecipitation of Native Chromatin: NChIP.” *Methods* 31 (1): 76–82. doi:10.1016/S1046-2023(03)00090-2.

Pellicelli, Martin, Julie A Miller, Alice Arabian, Claude Gauthier, Omar Akhouayri, Joy Y Wu, Henry M Kronenberg, and René St-Arnaud. 2014. “The PTH-Gαs-Protein Kinase A Cascade Controls αNAC Localization to Regulate Bone Mass.” *Molecular and Cellular Biology* 34 (9): 1622–33. doi:10.1128/MCB.01434-13.

Pittenger, M F, a M Mackay, S C Beck, R K Jaiswal, R Douglas, J D Mosca, M a Moorman, D W Simonetti, S Craig, and D R Marshak. 1999. “Multilineage Potential of Adult Human Mesenchymal Stem Cells.” *Science* 284 (5411): 143–47. doi:10.1126/science.284.5411.143.

Quélo, Isabelle, Claude Gauthier, Gregory E Hannigan, Shoukat Dedhar, and René St-Arnaud. 2004. “Integrin-Linked Kinase Regulates the Nuclear Entry of the c-Jun Coactivator Alpha-NAC and Its Coactivation Potency.” *The Journal of Biological Chemistry* 279 (42): 43893–99. doi:10.1074/jbc.M406310200.

Quélo, Isabelle, Josee Prud’homme, and René St-Arnaud. 2004. “GSK3β-Dependent Phosphorylation of the αNAC Coactivator Regulates Its Nuclear Translocation and

Proteasome-Mediated Degradation." *Biochemistry* 43 (10): 2906–14. doi:10.1021/bi036256.

Raggatt, Liza J, and Nicola C Partridge. 2010. "Cellular and Molecular Mechanisms of Bone Remodeling." *The Journal of Biological Chemistry* 285 (33): 25103–8. doi:10.1074/jbc.R109.041087.

Robinson, James T., Helga Thorvaldsdóttir, Wendy Winckler, Mitchell Guttman, Eric S. Lander, Gad Getz, Jill P. Mesirov. 2011. "Integrative Genomics Viewer." *Nature Biotechnology* 29, 24–26.

Sadowski, I, J Ma, S Triezenberg, and M Ptashne. 1988. "GAL4-VP16 Is an Unusually Potent Transcriptional Activator." *Nature* 335 (6190): 563–64.

Schmidt, Katy, Thorsten Schinke, Michael Haberland, Matthias Priemel, Arndt F Schilling, Cordula Mueldner, Johannes M Rueger, Elisabeth Sock, Michael Wegner, and Michael Amling. 2005. "The High Mobility Group Transcription Factor Sox8 Is a Negative Regulator of Osteoblast Differentiation." *The Journal of Cell Biology* 168 (6): 899–910. doi:10.1083/jcb.200408013.

Schmittgen, Thomas D, and Kenneth J Livak. 2008. "Analyzing Real-Time PCR Data by the Comparative CT Method." *Nature Protocols* 3 (6): 1101–8. doi:10.1038/nprot.2008.73.

Shimada, Takashi, and Makoto Kakitani. 2004. "Targeted Ablation of Fgf23 Demonstrates an Essential Physiological Role of FGF23 in Phosphate and Vitamin D Metabolism." *The Journal of Clinical Investigation* 113 (4): 561–68. doi:10.1172/JCI200419081.Introduction.

Smale, Stephen T. 2010. "Luciferase Assay." *Cold Spring Harbor Protocols* 2010 (5). doi:10.1101/pdb.prot5421.

Sommerfeldt, D W, and C T Rubin. 2001. "Biology of Bone and How It Orchestrates the Form and Function of the Skeleton." *European Spine Journal : Official Publication of the European Spine Society, the European Spinal Deformity Society, and the European Section of the Cervical Spine Research Society* 10 Suppl 2 (October): S86–95. doi:10.1007/s005860100283.

St-Arnaud, René, and Bahareh Hekmatnejad. 2011. "Combinatorial Control of ATF4-Dependent Gene Transcription in Osteoblasts." *Annals of the New York Academy of Sciences* 1237 (November): 11–18. doi:10.1111/j.1749-6632.2011.06197.x.

Sudo, H., H. a. Kodama, Y. Amagai, S. Yamamoto, and S. Kasai. 1983. "In Vitro Differentiation and Calcification in a New Clonal Osteogenic Cell Line Derived from Newborn Mouse Calvaria." *Journal of Cell Biology* 96 (1): 191–98. doi:10.1083/jcb.96.1.191.

Takeda, Shu, Florent Elefteriou, Regis Levasseur, Xiuyun Liu, Liping Zhao, Keith L Parker, Dawna Armstrong, Patricia Ducy, and Gerard Karsenty. 2002. "Leptin Regulates Bone Formation via the Sympathetic Nervous System." *Cell* 111 (3): 305–17. doi:10.1016/S0092-8674(02)01049-8.

Tam, C. S., J. N M Heersche, T. M. Murray, and J. a. Parsons. 1982. “Parathyroid Hormone Stimulates the Bone Apposition Rate Independently of Its Resorptive Action: Differential Effects of Intermittent and Continuous Administration.” *Endocrinology* 110 (2): 506–12. doi:10.1210/endo-110-2-506.

Teti, Anna. 2011. “Bone Development: Overview of Bone Cells and Signaling.” *Current Osteoporosis Reports* 9 (4): 264–73. doi:10.1007/s11914-011-0078-8.

Vondracek, Sheryl F. 2010. “Managing Osteoporosis in Postmenopausal Women.” *American Journal of Health-System Pharmacy : AJHP : Official Journal of the American Society of Health-System Pharmacists* 67 (7 Suppl 3): S9–19. doi:10.2146/ajhp100076.

Wan, Mei, Jun Li, Katie Herbst, Jin Zhang, Bing Yu, Xiangwei Wu, Tao Qiu, et al. 2011. “LRP6 Mediates cAMP Generation by G Protein-Coupled Receptors through Regulating the Membrane Targeting of Gα(s).” *Science Signaling* 4 (164): ra15. doi:10.1126/scisignal.2001464.

Wan, Mei, Chaozhe Yang, Jun Li, Xiangwei Wu, Hongling Yuan, Hairong Ma, Xi He, Shuyi Nie, Chenbei Chang, and Xu Cao. 2008. “Parathyroid Hormone Signaling through Low-Density Lipoprotein-Related Protein 6.” *Genes & Development* 22 (21): 2968–79. doi:10.1101/gad.1702708.

Wiedmann, B, H Sakai, TA Davis, and M Wiedmann. 1994. “A Protein Complex Required for Signal-Sequence-Specific Sorting and Translocation.” *Nature* 370: 434–40.

Wu, JY, Piia Aarnisalo, and Murat Bastepe. 2011. “Gsα Enhances Commitment of Mesenchymal Progenitors to the Osteoblast Lineage but Restrains Osteoblast Differentiation in Mice.” *The Journal of Clinical Investigation* 121 (9): 3492–3504. doi:10.1172/JCI46406DS1.

Yotov, Wagner V, Alain Moreau, and René St-Arnaud. 1998. “The Alpha Chain of the Nascent Polypeptide-Associated Complex Functions as a Transcriptional Coactivator The Alpha Chain of the Nascent Polypeptide-Associated Complex Functions as a Transcriptional Coactivator.” *Molecular and Cellular Biology* 18 (3): 1303–11.

Yotov, Wagner V, and Rene St-arnaud. 1996. “Differential Splicing-in of a Proline- Rich Exon Converts aNAC into a Muscle-Specific Transcription Factor.” *Genes & Development* 1: 1763–72.

Zhang, Chi. 2010. “Transcriptional Regulation of Bone Formation by the Osteoblast-Specific Transcription Factor Osx.” *Journal of Orthopaedic Surgery and Research* 5 (37). BioMed Central Ltd. doi:10.1186/1749-799X-5-37.

Zhang, Chi, Kyucheol Cho, Yehong Huang, Jon P Lyons, Xin Zhou, Krishna Sinha, Pierre D McCrea, and Benoit de Crombrugghe. 2008. “Inhibition of Wnt Signaling by the Osteoblast-Specific Transcription Factor Osterix.” *Proceedings of the National Academy of Sciences of the United States of America* 105 (19): 6936–41. doi:10.1073/pnas.0710831105.